Atom interferometers in weakly curved spacetimes using Bragg diffraction and Bloch oscillations

Michael Werner,[1] Philip K. Schwartz,[1] Jan-Niclas Kirsten-Siemß,[1,2] Naceur Gaaloul,[2] Domenico Giulini,[1,3] and Klemens Hammerer[1]

[1]*Institut für Theoretische Physik, Leibniz Universität Hannover, Appelstraße 2, 30167 Hannover, Germany*
[2]*Institut für Quantenoptik, Leibniz Universität Hannover, Welfengarten 1, 30167 Hannover, Germany*
[3]*Zentrum für Angewandte Raumfahrttechnologie und Mikrogravitation, Universität Bremen, Am Fallturm 1, 28359 Bremen, Germany*

(Received 18 October 2023; accepted 21 November 2023; published 29 January 2024)

We present a systematic approach to determine all relativistic phases up to $\mathcal{O}(c^{-2})$ in light-pulse atom interferometers in weakly curved spacetime that are based on elastic scattering—namely, Bragg diffraction and Bloch oscillations. Our analysis is derived from first principles using the parametrized post-Newtonian formalism. In the treatment developed here, we derive algebraic expressions for relativistic phases for arbitrary interferometer geometries in an automated manner. As case studies, we consider symmetric and antisymmetric Ramsey-Bordé interferometers, as well as a symmetric double diffraction interferometer with baseline lengths of 10 m and 100 m. We compare our results to previous calculations conducted for a Mach-Zehnder interferometer.

DOI: 10.1103/PhysRevD.109.022008

I. INTRODUCTION

Atom interferometers (IFs), at the forefront of quantum metrology, are highly precise instruments widely utilized in various research domains. They have been employed in diverse fields, including the determination of the fine-structure constant [1,2], serving as quantum sensors for measuring the gravitational field of the Earth [3–6], proposed measurements of gravitational waves [7–10], and investigations of fundamental physics and alternative gravitational models [11–15], as well as measurements of time dilation and gravitational redshift [16–20].

The interpretation of measurements of the gravitational redshift has ignited extensive discussions regarding the influence of relativistic effects in atom IFs [21–24]. These discussions have underscored the need for interferometry with internal superposition states [19,20] enabling the effective detection of gravitational redshift effects. As a result, there has been significant research focus on IFs employing inelastic scattering processes, such as single-photon or Raman transitions, commonly referred to as "clock interferometry." However, inelastic scattering introduces additional systematic effects due to the different internal atomic states. In contrast, atom IFs based on elastic scattering processes, such as Bragg diffraction [25,26] and Bloch oscillations [27,28], currently exhibit the highest sensitivity. This advancement has facilitated groundbreaking measurements, such as the precise determination of atomic recoil—and, consequently, the fine-structure constant—with unprecedented accuracy [2]. The gravitational redshift cannot be directly measured with these IFs; it is worth noting that phases involving relativistic effects and even extensions to the standard model (SME) can still manifest in these atom IFs [29,30].

Dimopoulos *et al.* [31,32] presented the determination and detailed listing of phases induced by special and general relativistic effects specifically for the Mach-Zehnder IF. However, the laborious algebraic calculations involved make it difficult to reproduce and extend these results to more general IF geometries. Here, we propose a systematic framework for computing relativistic phases in arbitrary atom IFs realized by elastic scattering. Our approach employs rigorous expansions in relevant small parameters, implemented through computer algebra in Python [33]. This enables automated algebraic calculations of relativistic phases up to the desired order of accuracy. We compute and display the phases for three common IF geometries: the symmetric Ramsey-Bordé interferometer (SRBI), antisymmetric Ramsey-Bordé interferometer (ARBI), and symmetric double diffraction interferometer (SDDI). The computer algorithm is, however, capable of calculating phases for more general IF geometries. For each geometry, we algebraically list and quantitatively illustrate the leading relativistic phases. Our analysis focuses on atom IFs with baseline lengths of 10 m and 100 m, inspired by numerous operational or under-development setups [10,34–38]. Furthermore, we provide a detailed comparison

to the results of Dimopoulos *et al.* [31,32] for the Mach-Zehnder IF, where we find overall good agreement and comment on the remaining discrepancies.

The starting point and basis of our calculation is a quantum optical Hamiltonian, as developed in [39]. It accounts for both the internal and external degrees of freedom of an atom, as well as the electromagnetic (EM) field, within a weak post-Newtonian gravitational background field which is described by the Eddington-Robertson parametrized post-Newtonian metric [40]. Consequently, this Hamiltonian captures the phases resulting from extensions of GR and provides a comprehensive description of the leading-order effects for scalar particles. Importantly, this treatment eliminates the need for additional relativistic corrections and avoids the requirement of *ad hoc* time reparametrization in the Schrödinger equation to account for time dilation, cf. the analysis of the mass defect in [41].

To achieve a self-consistent description of experiments that involve the measurement of time and length using local clocks and rulers—i.e., laser fields—we transform the Hamiltonian from the asymptotically flat coordinates, as formulated in [39], to coordinates which reduce to the Minkowski metric at a reference point—e.g., that of the experiment's reference atomic clock. This reformulation of the Hamiltonian holds significance not only for the description of atom IFs, but also for any other local experiments.

We begin in Sec. II by introducing the notation, explaining the gravitational model, and deriving the relativistically corrected Hamiltonian. We do this within the context of newly established coordinates, which are suitable for describing atom IFs. We continue in Sec. III to solve the Schrödinger equation for a general class of atom IF geometries which rely on elastic scattering. We then present the resulting phase shifts for the aforementioned IF geometries in Sec. IV. We end in Sec. V with a summary and conclusion. For improved readability, we supply intermediate calculation steps and supplemental information in Appendixes A–E.

II. RELATIVISTICALLY CORRECTED HAMILTONIAN OF AN ATOM IN WEAKLY CURVED SPACETIME

We adopt the following convention: greek indices range from 0 to 3, whereas latin indices range from 1 to 3. The components of the Minkowski metric are $\eta_{\mu\nu} = \mathrm{diag}(-1, 1, 1, 1)$. Bold letters like $\boldsymbol{x}$ and $\boldsymbol{R}$ will always represent three-dimensional quantities, like elements in $\mathbb{R}^3$ or 3-tuples of operators. Commas indicate partial differentiation, whereas semicolons abbreviate covariant derivatives—that is, $A_{\mu,\nu} = \partial_\nu A_\mu$ and $A_{\mu;\nu} = \nabla_\nu A_\mu$.

A. Gravitational model

We are going to model gravity by a *metric theory* in which test bodies follow geodesics with respect to the corresponding Levi-Civita connection and to which matter couples by the standard minimal scheme. In this way, Einstein's equivalence principle is implemented and spacetime is represented by the triple $(\mathcal{M}, g, \nabla)$, where $\mathcal{M}$ is a four-dimensional differentiable manifold, g a Lorentzian metric, and ∇ the corresponding Levi-Civita connection. This scheme may be extended to scalar-tensor [42] and vector-tensor theories [43], which we will not consider here.

To perform a Newtonian *weak field* and *slow motion* expansion of the physics in a relativistic spacetime, one first has to introduce a background structure with respect to which these notions can be defined [[44], Sec. 16.2.1]. This background structure we take to consist of a background metric and the worldline of a preferred observer. Then, one can implement the Newtonian expansion by a power series expansion in small parameters: the Newtonian gravitational potential $\phi/c^2 \ll 1$ and $v^2/c^2 \ll 1$, where v is a typical velocity of the matter sourcing gravity. With respect to the background structure, the metric tensor g then splits into the sum of (i) the background Minkowski metric, (ii) a first-order part describing Newtonian mechanics, and (iii) post-Newtonian corrections, special to each metric theory. This approach gives rise to a ten-parameter class of different metric theories and is described in the *parametrized post-Newtonian* (PPN) formalism [45]. The low-order post-Newtonian behavior of each metric theory is then uniquely determined by those ten *PPN parameters*.

In the following, we only consider two out of those ten possible parameters—namely, the "Eddington-Robertson (ER) parameters" $\beta, \gamma \in \mathbb{R}$, corresponding to the biggest relativistic corrections. In a local coordinate system $\mathsf{x}^\mu = \{c\mathsf{t}, \mathbf{r}\}$, the covariant PPN metric tensor components can, in the case of a spherically symmetric and static spacetime, be written using the line element

$$\mathrm{d}s^2 = -\left(c^2 + 2\phi(\mathbf{r}) + 2\beta\frac{\phi(\mathbf{r})^2}{c^2}\right)\mathrm{d}\mathsf{t}^2 + \left(1 - 2\gamma\frac{\phi(\mathbf{r})}{c^2}\right)\mathrm{d}\mathbf{r}^2 + \mathcal{O}(c^{-4}), \tag{1}$$

where the scalar field $\phi\colon \mathbb{R}^3 \to \mathbb{R}$ is the gravitational potential that arises from solving the Poisson equation [46]. In standard GR, the ER parameters are unity. Upper bounds for the ER parameters have long been known to be on the orders of $|\gamma - 1| \approx |\beta - 1| \lesssim 10^{-5}$, obtained by tracking, e.g., the trajectory of the Cassini mission or measuring perihelion shifts of Mercury and Mars (cf. [48–51]). We model Earth as a point source with mass $M_\oplus$—i.e., the Newtonian gravitational potential takes the form

$$\phi(\mathbf{r}) = -\frac{GM_\oplus}{|\mathbf{r}|}. \tag{2}$$

Notice that the metric tensor is asymptotically flat in these coordinates, since $\phi(\mathbf{r}) \to 0$ for $|\mathbf{r}| \to \infty$, which means that the metric tensor is not Minkowskian at the point of an earthbound experiment.

B. Transformation to adapted coordinates

Using coordinates in which the metric tensor asymptotically approximates the Minkowskian values makes asymptotic flatness manifest, but it also means that these coordinates cannot be employed for a direct representation of local measurements of spacetime distances in terms of simple coordinate expressions. Such measurements refer to colocated clocks and spatial length references set by light signals (e.g., by a laser). That itself would have to be described by a Hamiltonian operator, whereby the corresponding clock signal would contain the metric at the location of the experiment. In order to allow for a simpler and more direct interpretation of coordinates as quantities measurable with a local clock and length scale, it is convenient to transform to coordinates in which the metric components at the reference point of the experiment (set by clock and laser) reduce to the Minkowski metric.

The transformation from asympotically Minkowskian coordinates into such coordinates that we use is explained in Appendix A, and it is given by $(\mathsf{x}^\mu) = (c\mathsf{t}, \mathbf{r}) \mapsto (x^\mu) = (ct, \boldsymbol{r})$, with

$$t = \left(1 + \frac{\phi_0}{c^2} + \frac{2\beta - 1}{2}\frac{\phi_0^2}{c^4}\right)\mathsf{t}, \qquad \boldsymbol{r} = \left(1 - \gamma\frac{\phi_0}{c^2}\right)\mathbf{r}, \tag{3}$$

where we have defined $\phi_0 = \phi(\boldsymbol{R}_\oplus)$. Here, we assume the point of reference is at rest at Earth's surface—i.e., at a radius of $\boldsymbol{R}_\oplus$ in the new coordinates. It will be convenient to define the shifted gravitational potential

$$\bar{\phi}(\boldsymbol{r}) = \phi(\boldsymbol{r}) - \phi_0 \tag{4}$$

such that the line element in the new coordinates reads

$$\begin{aligned} \mathrm{d}s^2 = &-\left(c^2 + 2\bar{\phi} + 2\beta\frac{\bar{\phi}^2}{c^2} + 4(\beta - 1)\frac{\phi_0\bar{\phi}}{c^2}\right)\mathrm{d}t^2 \\ &+ \left(1 - 2\gamma\frac{\bar{\phi}}{c^2}\right)\mathrm{d}\boldsymbol{r}^2 + \mathcal{O}(c^{-4}), \end{aligned} \tag{5}$$

which reduces to the Minkowski metric for $\boldsymbol{r} = \boldsymbol{R}_\oplus$. This is the form of the metric that we shall use in the sequel.

C. Relativistically corrected Hamiltonian

The Hamiltonian for an atom, modeled as a system of two electromagnetically bound spinless point charges, coupled to an external EM field and the weakly curved PPN spacetime metric from Eq. (1), has been derived in [39]. We perform the same derivation as in [39] but use the coordinates from Eq. (3)—i.e., the metric tensor in Eq. (5). To zeroth order in $1/c^2$, this Hamiltonian corresponds to the standard description of an atom in nonrelativistic quantum optics. Terms of order $1/c^2$ correspond to the leading relativistic corrections to the energies of the center of mass and internal (electronic) degrees of freedom of the atom, as well as their mutual interactions and that with the external EM field. The Hamiltonian can be grouped as

$$\hat{H} = \hat{H}_\mathrm{M} + \hat{H}_\mathrm{I} + \hat{H}_\mathrm{M\text{-}I} + \hat{H}_\mathrm{A\text{-}L} + \mathcal{O}(c^{-4}). \tag{6}$$

It consists of the Hamiltonian for c.m. motion $\hat{H}_\mathrm{M}$, the Hamiltonian for the internal degrees of freedom $\hat{H}_\mathrm{I}$, their relativistic coupling $\hat{H}_\mathrm{M\text{-}I}$, and the relativistically corrected dipole interaction of the atom with the external EM field $\hat{H}_\mathrm{A\text{-}L}$. The external EM field is a classical solution to the source-free Maxwell equations in our curved spacetime [52]. In the following, the relativistically corrected canonical position and momentum operators of the c.m. and internal degrees of freedom will be denoted by $\hat{\boldsymbol{R}}, \hat{\boldsymbol{P}}$ and $\hat{\boldsymbol{r}}, \hat{\boldsymbol{p}}$, respectively. The total (rest) mass of the atom will be denoted by m, and the reduced mass of the internal degree of freedom by μ. The Hamiltonian for c.m. motion is

$$\hat{H}_\mathrm{M} = m\bar{\phi}(\hat{\boldsymbol{R}}) + \frac{\hat{\boldsymbol{P}}^2}{2m} \tag{7a}$$

$$+ \frac{1}{mc^2}\left[\frac{2\gamma + 1}{2}\hat{\boldsymbol{P}}\,\bar{\phi}(\hat{\boldsymbol{R}})\hat{\boldsymbol{P}} - \frac{\hat{\boldsymbol{P}}^4}{8m^2} + \frac{2\beta - 1}{2}m^2\bar{\phi}(\hat{\boldsymbol{R}})^2\right] \tag{7b}$$

$$+ 2(\beta - 1)m^2\phi_0\bar{\phi}(\hat{\boldsymbol{R}})\Big] + \mathcal{O}(c^{-4}). \tag{7c}$$

The terms in the square brackets—i.e., Eqs. (7b) and (7c)—comprise the relativistic corrections of the c.m. energy, and they will be the most relevant for our analysis. The first of those terms corresponds to the metric correction of the length of the vector $\hat{\boldsymbol{P}}$ determining the kinetic energy, written in symmetric ordering. The second term is the special relativistic correction to the kinetic energy, the third term describes the relativistic nonlinear correction to the Newtonian potential, and the final term represents nonlinear relativistic effects which may arise in theories of gravity deviating from GR.

The internal Hamiltonian,

$$\hat{H}_\mathrm{I} = \frac{\hat{\boldsymbol{p}}^2}{2\mu} - \frac{e^2}{4\pi\epsilon_0|\hat{\boldsymbol{r}}|} + H_\mathrm{FS}, \tag{8}$$

consists of the nonrelativistic kinetic energy and Coulomb interaction and relativistic corrections subsumed in the fine-structure Hamiltonian H_FS, which contains the special relativistic corrections of kinetic and Coulomb energy,

as well as spin-orbit interaction, etc., if spin was included. We refer to [39] for the explicit form of H_{FS}. In the following, we take these corrections to be accounted for in the internal stationary states and energies—e.g., the ground state $\hat{H}_{\mathrm{I}}|g\rangle = E_g|g\rangle$.

The relativistic coupling of the c.m. and internal degrees of freedom has the form

$$\hat{H}_{\mathrm{M\text{-}I}} = \frac{1}{mc^2}\left(m\phi(\hat{\boldsymbol{R}}) - \frac{\hat{\boldsymbol{P}}^2}{2m}\right) \otimes \hat{H}_{\mathrm{I}} + \frac{\phi(\hat{\boldsymbol{R}})}{c^2} \otimes \left(2\gamma\frac{\hat{\boldsymbol{p}}^2}{2\mu} - \gamma\frac{e^2}{4\pi\epsilon_0|\hat{\boldsymbol{r}}|}\right). \tag{9}$$

The first line of this equation can be interpreted as arising from the correction of the mass of the atom due to internal binding energy, as can be seen by replacing $m \to m + \hat{H}_{\mathrm{I}}/c^2$ in Eq. (7a) and expanding in $1/c^2$. The second line describes the metric corrections of the internal kinetic and Coulomb energy, similar to Eqs. (7b) and (7c), cf. [44]. For atom IFs involving elastic scattering processes only, the atom remains in its internal ground state $|g\rangle$ at all times. In this case, the terms in Eq. (9) contribute only trivially to the dynamics of the problem: As explained above, the effect of the first term can be absorbed in a rescaling of the atomic mass $m \to m + E_g/c^2$. The second term does not contribute at all, since it has vanishing matrix elements for stationary states [41] as a consequence of the virial theorem [54]. However, they can be the main contribution to the phase in quantum clock IFs with inelastic scattering processes [19,20,55,56].

Finally, the Hamiltonian for the interaction of the atom with the external light field is

$$\hat{H}_{\mathrm{A\text{-}L}} = -\hat{\boldsymbol{d}}\cdot\boldsymbol{E}^{\perp}(\hat{\boldsymbol{R}}) + \frac{1}{2m}[\hat{\boldsymbol{P}}\cdot(\hat{\boldsymbol{d}}\times\boldsymbol{B}(\hat{\boldsymbol{R}})) + \mathrm{H.c.}], \tag{10}$$

where $\hat{\boldsymbol{d}}$, $\boldsymbol{E}$, and $\boldsymbol{B}$ denote the dipole moment operator and the electric and magnetic fields, respectively. The atom-light interaction in Eq. (10) is written in the dipole approximation and includes the Röntgen term as the dominant relativistic correction [57]. In comparison to the Hamiltonian from [39], only the last term in the motional Hamiltonian—i.e., Eq. (7c)—is a new contribution. Its specific scaling with the PPN parameter β is commented on in Appendix A. Apart from this new term, the only difference is the dependence on $\bar{\phi}$ instead of ϕ.

We note that a physical misinterpretation of the coordinates used in Eq. (1) easily results in erroneous terms scaling with ϕ_0/c^2, as was the case, e.g., in the debate about such contributions in the measurements of the electronic gyromagnetic factor g_e [58–60]. Such pitfalls can be avoided by working in the coordinates in Eq. (3), where the Hamiltonian in Eq. (6) has no dependence at all on ϕ_0 for GR ($\beta = 1$).

III. ATOM INTERFEROMETERS USING ELASTIC SCATTERING

In this section, we solve the Schrödinger equation for a range of IF geometries, which involve elastic scattering processes. We illustrate our approach using three specific atom IF geometries, shown in Fig. 1. We will consider c.m. motion along the vertical direction. In the following, we denote the vertical coordinate—i.e., that pointing (radially) upwards in Earth's gravitational field—by Z. For the earth-bound IF geometries considered in the following, we assume height differences ΔZ on the order of 10 m, as realized in [36,61,62], up to several 100 m baselines, as currently under investigation [37,38]. Therefore, it will be appropriate to expand the gravitational potential at height Z above ground as

$$\phi|_{\mathrm{height}\,Z} = \phi_0 + gZ - \frac{1}{2}\Gamma Z^2 + \frac{1}{3}\Lambda Z^3, \tag{11}$$

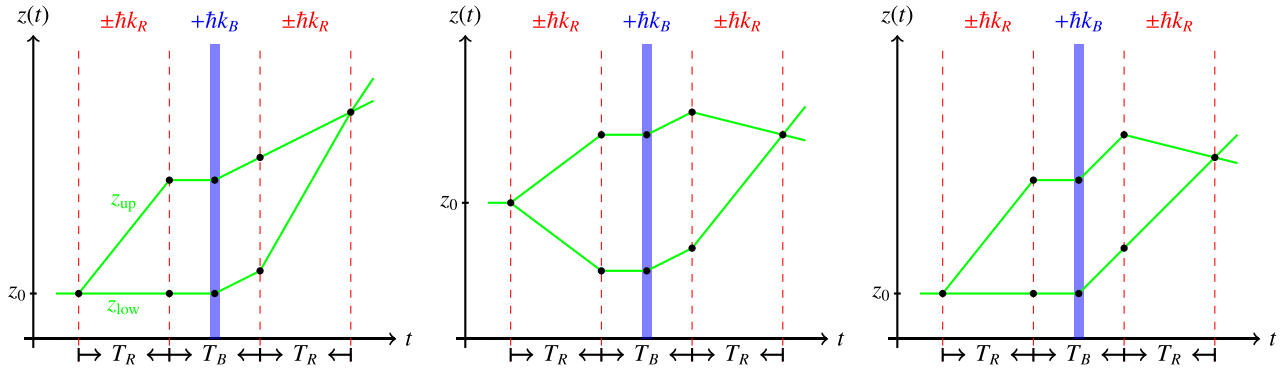

FIG. 1. Schematic pictures of atomic trajectories (green lines) for three different IF geometries in the freely falling frame. Bragg pulses are depicted in red dashed lines with a momentum transfer of $\pm\hbar k_R$ and Bloch oscillations in solid blue with a momentum transfer of $\hbar k_B$. Finite-speed-of-light effects are neglected in this picture. (a) Symmetric Ramsey-Bordé Interferometer (SRBI), (b) Symmetric Double Diffraction Interferometer (SDDI), (c) Asymmetric Ramsey-Bordé Interferometer (ARBI). Note that (a) and (c) can be realized using single Bragg diffraction, whereas (b) relies on double Bragg diffraction.

with ϕ_0 as before, linear gravitational acceleration g, gravity gradient Γ, and the second-order gradient Λ. We choose to expand $\phi(\boldsymbol{r})$ to third order to facilitate a comparison of our results with Refs. [31,32]. It also allows us to include gravitational effects from other source masses, either due to test masses as in Refs. [63,64] or due to mass inhomogeneities, such as those studied for the Very Long Baseline Atom Interferometer (VLBAI) [65]. Using this expansion, the Hamiltonian in Eq. (7) for c.m. motion along the vertical axis becomes

$$\begin{aligned}\hat{H}_{\mathrm{M}} = {} & mg\hat{Z} - \frac{m}{2}\Gamma\hat{Z}^2 + \frac{m}{3}\Lambda\hat{Z}^3 + \frac{\hat{P}^2}{2m} \\ & + \frac{1}{mc^2}\left[\frac{2\gamma+1}{2}g\hat{P}\,\hat{Z}\,\hat{P} - \frac{\hat{P}^4}{8m^2} + \frac{2\beta-1}{2}m^2g^2\hat{Z}^2\right. \\ & \left. + 2(\beta-1)m^2\phi_0 g\hat{Z}\right] + \mathcal{O}(\Gamma c^{-2}). \end{aligned} \tag{12}$$

In the IF geometries considered here, we assume atoms are initialized in a wave packet which is localized at coordinate height z_0 and has vertical coordinate velocity v_0. The IF sequences consist in each case of an initial and a final light pulse splitting and recombining the wave packet in momentum by Bragg diffraction. After the first beam splitter, a free propagation for a (Ramsey) time T_R and another Bragg pulse, we consider a time T_B in which (optional) Bloch oscillations accelerate both wave packet components. Subsequently, the atoms, again, interact with a Bragg pulse, propagate freely for a time T_R, after which the wave packet is recombined in a final Bragg pulse. The time decomposition (T_R, T_B, T_R) is chosen symmetrically to obtain compact final results, yet it is in principle straightforward to describe asymmetrical pulse sequences. This general class of IF geometries corresponds to the SRBI and ARBI like in [16] with intermediate Bloch oscillations, as performed in the fine-structure measurements [1,2], and a similar geometry using double Bragg diffraction [66,67]. These example IF geometries can be considered as representatives of different IF classes that exhibit different symmetry axes. Investigating how the different symmetries are reflected in the phase shift results might then be an interesting study in the future.

In solving the Schrödinger equation for geometries and pulse sequences as shown in Fig. 1, we approximate the light pulses as instantaneous on the scale of the Ramsey time T_R [68]. Relativistic contributions to phases imparted during the free propagation times T_R will be evaluated in Sec. III A, and those due to the Bragg pulses in Sec. III C. Finally, we assume that phases imprinted by the Bloch pulses are common mode and therefore do not contribute to the IF signal. Accounting for differential phases (due to gravity gradients or relativistic corrections) accumulated during Bloch pulses is beyond the scope of this work.

A. Free propagation

During free propagation, the atoms remain in the ground state $|g\rangle$, and we need to solve the Schrödinger equation with the Hamiltonian in Eq. (12) for the c.m. wave function $\psi(z,t)$. For wave packets which stay localized around the classical trajectories corresponding to the IF paths in Fig. 1, it is sufficient to determine the *propagation phase*—i.e., the relative phase accumulated along the two paths. Following the stationary phase approximation, one can approximate the propagation phase by the difference of the action functional along the upper trajectory $z_{\mathrm{up}}(t)$ and the lower trajectory $z_{\mathrm{low}}(t)$ [69,70]:

$$\Delta\Phi_{\mathrm{Prop}} = \frac{1}{\hbar}\int [L_{\mathrm{M}}(z_{\mathrm{up}}(t)) - L_{\mathrm{M}}(z_{\mathrm{low}}(t))]\mathrm{d}t. \tag{13}$$

Here, L_{M} is the Lagrangian corresponding to Eq. (12), whose explicit form can be found in Appendix B. We point out that Eq. (13) for the propagation phase only applies exactly for Lagrange functions, which depend quadratically on position and velocity. For a more general Lagrangian [cf. Eq. (B1)], however, Eq. (13) only applies under a stationary phase approximation. In the following, we will perform a systematic expansion of the propagation phase with respect to the small, nonquadratic terms of the Lagrangian. Corrections beyond the stationary phase approximation would only contribute in a higher and negligibly small order.

In order to find the classical trajectories of the upper and lower arms of the IF, we need to solve the geodesic equation, or equivalently, the Euler-Lagrange equation (ELE) corresponding to Eq. (12), which is given explicitly in Appendix B. Rather than seeking the exact trajectories, we construct approximate solutions of the ELE which are accurate in leading orders of Γ, Λ, and c^{-1}. These approximations can be performed systematically by rewriting the ELE in a dimensionless form in terms of scaled time and position variables:

$$\tau = \frac{t}{T_R}, \qquad \xi(\tau) = \frac{z(\tau)}{cT_R}. \tag{14}$$

Here, we choose T_R as the natural timescale of the IF sequences under consideration. In terms of these new variables, the ELE depends on a number of dimensionless parameters, summarized in Table I. They are connected to the gravitational potential, initial conditions for the atomic wave packet, and momentum recoils from light pulses. In terms of the dimensionless variables τ and ξ and the dimensionless parameters of Table I, the ELE reads

$$\begin{aligned}\ddot{\xi}(\tau) = {} & -\mathcal{G}_{1,\mathrm{R}} + \mathcal{G}_{2,\mathrm{R}}\xi(\tau) - \mathcal{G}_{3,\mathrm{R}}\xi(\tau)^2 \\ & - 2(\beta+\gamma)\mathcal{G}_{1,\mathrm{R}}^2\xi(\tau) + (\gamma+2)\mathcal{G}_{1,\mathrm{R}}\dot{\xi}(\tau)^2 \\ & + 2(\beta-1)\mathcal{G}_0[-\mathcal{G}_{1,\mathrm{R}} + \mathcal{G}_{2,\mathrm{R}}\xi(\tau)] + \mathcal{O}(4), \end{aligned} \tag{15}$$

TABLE I. Definitions of dimensionless parameters for an atom IF based on elastic scattering processes. As a case study, we give the magnitudes for a 10 m baseline Rb IF assuming the following values: $T_R = 1.3$ s, $T_B = 0.4$ s, $z_0 = 0$, $v_0 = 13$ m/s, $m = 87$ u, $\omega_R = 10^7$ Hz, $k_R = 16 \times 10^6$ m^{-1}, and $k_B = 5 \times 10^8$ m^{-1}.

		Magnitude for 10 m baseline IF	
Parameter	Definition	$i = R$ (Bragg)	$i = B$ (Bloch)
$\mathcal{Z}_0$	$\frac{z_0}{cT_R}$	0	
$\mathcal{V}_0$	$\frac{v_0}{c}$	4.3×10^{-8}	
$\mathcal{F}_\mathrm{R}$	$\frac{\hbar\omega_R}{mc^2}$	8.1×10^{-20}	
$\mathcal{G}_0$	$\frac{\phi_0}{c^2}$	7×10^{-10}	
$\mathcal{G}_{1,i}$	$\frac{gT_i}{c}$	4.2×10^{-8}	1.3×10^{-8}
$\mathcal{G}_{2,i}$	ΓT_i^2	5.2×10^{-6}	4.9×10^{-7}
$\mathcal{G}_{3,i}$	$\Lambda c T_i^3$	4.8×10^{-4}	1.4×10^{-5}
$\mathcal{R}_i$	$\frac{\hbar k_i}{mc}$	3.9×10^{-11}	1.2×10^{-9}

as shown in Appendix B. Throughout this manuscript, we use the notation $\mathcal{O}(n)$ to collect terms which are at least of nth order in the small dimensionless parameters in Table I. If we denote each time instance of light-matter interactions along the paths by τ_i with $i \in \mathbb{N}$, as indicated by the black dots in Fig. 1, we can define $\xi(\tau)$ piecewise by a set of functions $\xi_i(\tau)$ on the time intervals $[\tau_i, \tau_{i+1})$. A unique solution therefore requires the knowledge of two initial conditions for each segment of propagation. They can be constructed iteratively for $i > 0$ via

$$\xi_i(\tau_i) = \xi_{i-1}(\tau_i), \tag{16a}$$

$$\dot{\xi}_i(\tau_i) = \dot{\xi}_{i-1}(\tau_i) + N_R^{(i)}\mathcal{R}_\mathrm{R} + N_B^{(i)}\mathcal{R}_\mathrm{B}, \tag{16b}$$

whereas the first two initial conditions are

$$\xi_0(\tau_0) = \mathcal{Z}_0, \quad \dot{\xi}_0(\tau_0) = \mathcal{V}_0 + N_R^{(0)}\mathcal{R}_\mathrm{R} + N_B^{(0)}\mathcal{R}_\mathrm{B}. \tag{17}$$

$N_R^{(i)}$ and $N_B^{(i)}$ denote the number of photon recoils imprinted at time τ_i via the Bragg or Bloch interactions, respectively, and will be discussed later. The dot in Eq. (16) indicates differentiation with respect to τ. Note that $\mathcal{Z}_0$ denotes the initial height of the atoms compared to the reference position of the laser/clock; see Sec. II B. This parameter can be significant in differential measurements between different IFs—as, for example, in UFF tests, where an uncertainty of the relative difference in initial height will lead to relevant phase contributions [71]. Despite its implementation in our algorithm [33], we set $\mathcal{Z}_0 = 0$ in the following for simplicity.

Using the example of a drop tower with 10 m height, we show in Table I that the dimensionless parameters are small in the case of the IFs in Fig. 1. We exploit this fact to consistently construct an approximate solution of the ELE. For example, the trajectory of the path segment starting at τ_0, up to second order in these small parameters, is given by

$$\xi(\tau) = \xi(\tau_0) + \dot{\xi}(\tau_0)\tau - \frac{1}{2}(1 + 2(\beta - 1)\mathcal{G}_0)\mathcal{G}_{1,\mathrm{R}}\tau^2 + \frac{\mathcal{G}_{2,\mathrm{R}}}{2}\left(\xi(\tau_0)\tau^2 + \frac{1}{3}\dot{\xi}(\tau_0)\tau^3 - \frac{1}{12}\mathcal{G}_{1,\mathrm{R}}\tau^4\right) + \mathcal{O}(3). \tag{18}$$

Note that corrections induced by the third-order expansion of the gravitational potential—i.e., $\mathcal{G}_{3,\mathrm{R}}$—would only manifest at $\mathcal{O}(3)$. With this solution strategy, we calculate each of the IF paths—i.e., $\xi_\mathrm{up}(\tau)$ and $\xi_\mathrm{low}(\tau)$ for all three IF geometries. The propagation phase in Eq. (13) can now be calculated in dimensionless form using those trajectories:

$$\Delta\Phi_\mathrm{Prop} = \omega_\mathrm{C} T_R \int \left[\frac{L_\mathrm{M}(\xi_\mathrm{up}(\tau))}{mc^2} - \frac{L_\mathrm{M}(\xi_\mathrm{low}(\tau))}{mc^2}\right] \mathrm{d}\tau, \tag{19}$$

where we introduce the atomic Compton frequency

$$\omega_\mathrm{C} = \frac{mc^2}{\hbar}. \tag{20}$$

The propagation phase has to be consistently expanded in terms of the small dimensionless parameters up to the desired order. If the trajectory is known to $\mathcal{O}(2)$, one can calculate the propagation phase to $\mathcal{O}(3)$, since the Lagrangian depends on the velocity to second order and on the trajectory to first order after multiplication with $\mathcal{G}_{1,\mathrm{R}}$ and additional higher-order terms; see Appendix B for details. Similarly, the propagation phase can be evaluated to $\mathcal{O}(4)$ by first determining the trajectory to order $\mathcal{O}(3)$. The required integrals over the segments of the full IF sequence are in principle straightforward, but they result in tedious and error-prone calculations. We perform these calculations to $\mathcal{O}(4)$ using computer algebra based on SYMPY in Python [33]. The results for trajectories are too lengthy to be reproduced here, but they are given in [33].

So far, we have only considered the propagation phase in Eq. (19). However, taking into account the gravity gradient Γ and its spatial derivative Λ, one encounters the problem that the IF will not exactly close at the output port without special mitigation schemes [72–74]. In this case, one also has to take into account the *separation phase*, which is usually obtained by taking the spatial separation at the output port multiplied by the average momentum of the two atomic ports [32,75]. Writing directly in terms of the dimensionless trajectory from before, we can denote the output port separation as $\Delta\xi = \xi_\mathrm{l}(\tau_\mathrm{f}) - \xi_\mathrm{u}(\tau_\mathrm{f})$ and the average output velocity as $\dot{\xi}_\mathrm{aver} = \frac{1}{2}(\dot{\xi}_\mathrm{l}(\tau_\mathrm{f}) + \dot{\xi}_\mathrm{u}(\tau_\mathrm{f}))$, such that the separation phase can be written as

$$\Delta\Phi_\mathrm{Sep} = \omega_\mathrm{C} T_R \Delta\xi \cdot \dot{\xi}_\mathrm{aver}. \tag{21}$$

The quantities $\Delta\xi$ and $\dot{\xi}_{\text{aver.}}$ need to be evaluated to the desired order to obtain the separation phase. Since trajectory separations only appear due to nonlinear gravitational effects, which manifests at second order in the trajectory, one should note that $\Delta\xi$ is also at least $\mathcal{O}(2)$ in the absence of any mitigation schemes [72]. Since $\dot{\xi}_{\text{aver.}}$ is an $\mathcal{O}(1)$ term, the separation phase overall is of $\mathcal{O}(3)$. Additional relativistic $\mathcal{O}(c^{-2})$ corrections to $\Delta\Phi_{\text{Sep}}$ will be at least of order $\mathcal{O}(5)$; see Table I.

Note that due to the finite speed of light (FSL), the interaction times between the upper and lower interferometry paths will differ slightly and therefore alter the integration times in the propagation phase. FSL effects like those arise naturally at $\mathcal{O}(c^{-1})$—i.e., any additional gravitational effects would manifest at $\mathcal{O}(c^{-3})$. Furthermore, FSL-related effects are highly dependent on the actual experimental realization. In particular, they are determined by the initial laser positions, additional mirrors, or other optical elements. The calculation of FSL effects thus requires various experiment-specific parameters, each of which would significantly complicate the notation presented here. Conversely, assuming constraints on FSL effects and light paths requires selecting specific experimental configurations, contradicting our goal to provide a general framework. This is why, for now, we have chosen to omit FSL terms. However, we will compare our results to the Mach-Zehnder IF from [32] in Appendix E and demonstrate how to add the dominant FSL phases, in the case of an explicitly given experimental setup, by hand. We refer the interested reader to the paper of Tan *et al.* [76] analyzing contributions of FSL effects in a very general context, as well as to [56,77] for direct applications in atom IFs. An implementation of the full FSL effect into our algorithm for given experimental setups is going to be addressed in future work.

B. Maxwell equations in gravity

Following Refs. [32,78], so far we have considered only relativistic corrections of atomic degrees of freedom. Now, we proceed to analyze the EM field and its interaction with atoms in the PPN curved spacetime. The logic here will be to first identify the eigenmodes of the relativistically corrected wave equation for the light field, and then in the next section to use these when describing the interaction of atoms with a coherent laser field in a semiclassical approximation—namely, considering a coherent laser field in (some of) these eigenfunctions coupled to an atom via $H_{\text{A-L}}$ in Eq. (10). An approach that is similar to ours has been taken in [30].

The most straightforward way to obtain the Maxwell equations in general coordinates is to start from the Lagrangian and use the variational principle. The Lagrangian for an EM field in vacuum with the EM field strength tensor $F_{\mu\nu}$ is given by

$$L_{\text{L}} = \int \frac{\sqrt{-g}}{4\mu_0} F_{\mu\nu}F^{\mu\nu}\mathrm{d}^3\boldsymbol{x}, \tag{22}$$

where g is the determinant of the matrix of spacetime metric components, and the field strength tensor is taken as derived from a vector potential A_μ via $F_{\mu\nu} = A_{\nu;\mu} - A_{\mu;\nu} = A_{\nu,\mu} - A_{\mu,\nu}$ (thus, the homogeneous Maxwell equations $\mathrm{d}F = 0$, or in components, $F_{[\mu\nu;\rho]} = F_{[\mu\nu,\rho]} = 0$, are automatically satisfied). The variational principle, varying with respect to A_μ, then directly leads to the inhomogeneous Maxwell equations (in our case, with vanishing source):

$$F^{\alpha\beta}{}_{;\beta} = 0. \tag{23}$$

We solve Eq. (23) in Lorenz gauge $A_\mu{}^{;\mu} = 0$; see Appendix C for details. Note that for the solutions of interest to us and to our order of approximation, the Lorenz gauge agrees with the curved-spacetime generalization $A_i{}^{;i} = 0$ of the Coulomb gauge. The solution for a light field propagating in the z direction results in a geometric optics approximation of the potential A_μ with $A_0 = 0$ and a covariant spatial part $\boldsymbol{A} = (A_i)_i$ of the form

$$\boldsymbol{A} = \boldsymbol{\mathcal{A}} e^{\mathrm{i}\Phi(z,t)} + \mathcal{O}(\Gamma c^{-2}). \tag{24}$$

Here, $\boldsymbol{\mathcal{A}} = (\mathcal{A}_x, \mathcal{A}_y, 0)$ are the amplitudes and

$$\Phi(z,t) = k_0 ct \pm \left(1 - \frac{\gamma+1}{2}\frac{gz}{c^2}\right) k_0 z + \mathcal{O}(\Gamma c^{-2}) \tag{25}$$

is the phase of the EM field, where the sign depends on the direction of propagation. k_0 is the zeroth component of the covariant 4-wave-vector, and we have omitted dependencies on the transverse coordinates x, y in a plane wave approximation. The derivation of Eqs. (24) and (25) can be found in Appendix C.

The effective wave vector of the EM field in the relevant $(1+1)$-dimensional (ct, z) spacetime is

$$\begin{aligned}(k_\mu(z)) &= (\partial_\mu \Phi(z,t)) \\ &= \begin{pmatrix} 1 \\ \pm\left(1 - (\gamma+1)\frac{gz}{c^2}\right) \end{pmatrix} k_0 + \mathcal{O}(\Gamma c^{-2}).\end{aligned} \tag{26}$$

We note that the component k_0 is a coordinate-dependent quantity and has, *a priori*, no direct physical meaning. To interpret k_0, one needs to convert it into a measurable frequency, which requires the notion of a local observer. For this, we consider an observer resting at height z above Earth's surface, defined by its 4-velocity $(u^\mu_{\text{obs}}(z))$. Since 4-velocities are normalized to $u^\mu u_\mu = -c^2$, it follows that

$$(u^\mu_{\text{obs}}(z)) = \left(1 - \frac{gz}{c^2} + \mathcal{O}(\Gamma c^{-2})\right)\begin{pmatrix} c \\ 0 \end{pmatrix}. \tag{27}$$

The frequency of the light field as measured by this observer at rest at height z is then

$$\omega(z) = -k_\mu(z) u^\mu_{\text{obs}}(z) = -\left(1 - \frac{gz}{c^2} + \mathcal{O}(\Gamma c^{-2})\right) c k_0, \tag{28}$$

which may be interpreted as the gravitational redshift as witnessed by observers at rest at different heights. In the following, we will assume that this observer is located at $z = 0$ and equipped with a clock and a laser of frequency $\omega_0 = \omega(0)$, such that $k_0 = -\frac{\omega_0}{c}$. One may think here of an atomic clock and a laser which is stabilized to its reference frequency.

C. Light-matter interactions and the laser phase

We are now in a position to analyze the atom-light interaction in order to describe beam splitter and mirror pulses including relativistic corrections. Coming back to the interaction Hamiltonian in Eq. (10), we see that there are no direct gravitational effects apparent on the Hamiltonian level. However, since the EM fields themselves are gravitationally altered, we need to analyze how those corrections might affect beam splitter and mirror pulses.

1. Bragg interactions: Two counterpropagating light fields

We start by considering relativistically altered Bragg transitions which realize the mirror and beam splitter operations in Fig. 1. For this, we will describe the two counterpropagating light beams aligned in the z direction. The light fields are assumed to have frequencies $\omega_{R,1}$ and $\omega_{R,2}$ and wave vectors $k_{R,i} = \frac{\omega_{R,i}}{c} > 0$. We denote the "effective" frequency and wave vector as $\omega_R = \omega_{R,1} - \omega_{R,2}$ and $k_R = k_{R,1} + k_{R,2}$ and assume that those parameters induce a resonant two-photon process. The index R refers to the Ramsey sequence opened and closed by Bragg pulses, cf. Fig. 1, and follows the notation used, e.g., by Morel *et al.* [1]. Later on, in Sec. III C 4, we will also consider light pulses transferring the momentum k_B via Bloch oscillations.

In principle, the dynamics during a light pulse requires us to solve the Schrödinger equation with the Hamiltonian in Eq. (10), which reads in one-dimensional form

$$\hat{H}_{\text{A-L}} = -\hat{\boldsymbol{d}} \cdot \hat{\boldsymbol{E}}(\hat{Z}) + \frac{1}{2m}[\hat{P}(\hat{\boldsymbol{d}} \times \hat{\boldsymbol{B}}(\hat{Z}))_z + \text{H.c.}], \tag{29}$$

with position and momentum operators $\hat{Z}$, $\hat{P}$. This calculation is deferred to Appendix D, and we only summarize its result in the following. We first discuss the case of atoms at rest and include effects due to Doppler shifts in a second step. The $\hat{Z}$ dependence of the EM fields, which follow from the vector potential in Eq. (24), result in $\hat{Z}$-dependent corrections to the EM phases. This height dependence of the phase will be of relevance for the net interferometric phase and will be the focus in the following.

The wave vector of each laser will be gravitationally altered according to

$$\kappa_i(z) = \pm\left(1 - (\gamma + 1)\frac{gz}{c^2}\right) k_{R,i} + \mathcal{O}(\Gamma c^{-2}). \tag{30}$$

Hence, in order to achieve a resonant transition, we aim to transfer only the desired momentum of $k_{R,i}$ upon interaction. One therefore needs to detune each laser such that $\kappa(z_{\text{int}}) = \pm k_{R,i}$, where z_{int} is the interaction height between the light pulse and (a component of) the atomic wave packet on the respective path—i.e., $k_{R,i} \mapsto (1 + (\gamma + 1)\frac{gz_{\text{int}}}{c^2}) k_{R,i}$.

The effective laser phase imprinted on the atoms in a two-photon process at the interaction height z_{int} is given by

$$\Phi_L(z_{\text{int}}) = \pm\left(1 + \frac{\gamma + 1}{2}\frac{gz_{\text{int}}}{c^2}\right) k_R z_{\text{int}} + \Phi_{\text{FSL}} + \mathcal{O}(\Gamma c^{-2}), \tag{31}$$

where the sign corresponds to a net gain or loss in momentum, respectively. We absorb FSL effects in Φ_{FSL} and refer to Appendix D for details.

As shown in Appendix D, the scattering matrix for a Bragg diffraction transferring a momentum $N\hbar k_R$ reads

$$U^{(\theta)}(z_{\text{int}}) = \frac{1}{\sqrt{2}} \begin{pmatrix} \cos(\theta) & \mathrm{i}\sin(\theta) e^{\mathrm{i}N\Phi_L(z_{\text{int}})} \\ \mathrm{i}\sin(\theta) e^{-\mathrm{i}N\Phi_L(z_{\text{int}})} & \cos(\theta) \end{pmatrix} \tag{32}$$

in the basis of the momentum eigenstates $|0\hbar k_R\rangle$ and $|N\hbar k_R\rangle$. In the experiment, the angle θ is controlled via pulse intensities and durations [79,80] and is tuned to $\pi/2 + n\pi$ for a beam splitter and $\pi + 2n\pi$ for a mirror pulse with $n \in \mathbb{Z}$. Note that due to the various relativistic effects in the Rabi frequency and the detuning, this angle θ will, in principle, also depend on position and momentum, but at an insignificant level, as argued above.

2. Doppler effect and laser phase

To address the Doppler effect, we must examine the frequencies of the two light fields in the atoms' rest frame. Assuming that the atoms have a velocity of v_{int} upon interacting with these light fields, we can deduce that the atoms will undergo both first- and second-order Doppler shifts, as detailed in Appendix D. In order to compensate this shift, one needs to, similarly to the gravitational detuning before, rescale the laser frequencies beforehand, according to

$$\omega_{R,1} \mapsto \left(1 + \frac{v_{\text{int}}}{c} - \frac{v_{\text{int}}^2}{2c^2}\right)\omega_{R,1}, \tag{33a}$$

$$\omega_{R,2} \mapsto \left(1 - \frac{v_{\text{int}}}{c} - \frac{v_{\text{int}}^2}{2c^2}\right)\omega_{R,2}. \tag{33b}$$

The atoms then interact with light fields of appropriate frequencies—i.e., $\omega_{R,i}$, as measured in their own frame of reference—in order to resonantly stimulate the desired two-photon transition with a momentum kick of $\hbar k_R$. From this point onward, consider the frequencies $\omega_{R,i}$ as the values already detuned as described in Eq. (33). The imprinted phase [Eq. (31)] will then be additionally Doppler shifted and is given by

$$\Phi_L(z_{\rm int}, v_{\rm int}) = \pm\left(k_R + \frac{v_{\rm int}}{c}\frac{\omega_R}{c} - \frac{v_{\rm int}^2}{2c^2}k_R + \frac{\gamma+1}{2}\frac{g z_{\rm int}}{c^2}k_R\right) z_{\rm int} + \mathcal{O}(\Gamma c^{-2}), \quad (34)$$

where we have suppressed the FSL correction. For later reference, we rewrite each laser phase contribution in Eq. (34) in a dimensionless form, similar to the propagation phase Eq. (19) and the separation phase Eq. (21):

$$\Phi_L(\xi_{\rm int}, \dot{\xi}_{\rm int}) = \pm\omega_{\rm C} T_R\left(\left(1 - \frac{\dot{\xi}_{\rm int}^2}{2} + \frac{\gamma+1}{2}\mathcal{G}_{1,\rm R}\xi_{\rm int}\right)\mathcal{R}_{\rm R} + \dot{\xi}_{\rm int}\mathcal{F}_{\rm R}\right)\xi_{\rm int} + \mathcal{O}(5), \quad (35)$$

where we have again used the Compton frequency from Eq. (20). The Doppler term proportional to $\mathcal{F}_{\rm R}$ and the recoil term proportional to $\mathcal{R}_{\rm R}$ make contributions to the laser phases of $\mathcal{O}(3)$ and $\mathcal{O}(4)$, respectively. The terms of $\mathcal{O}(\Gamma c^{-2})$ in Eq. (34) translate to order $\mathcal{O}(5)$. We therefore aim to correctly determine each phase shift contribution consistently to $\mathcal{O}(4)$.

In summary, the overall *relative* laser phase accumulated along the upper and lower IF paths $\xi_{\rm up}(\tau)$ and $\xi_{\rm low}(\tau)$, also referred to as the kick phase [16], is

$$\Delta\Phi_{L,R} = \sum_i \left(\Phi_L(\xi_{\rm up}(\tau_i), \dot{\xi}_{\rm up}(\tau_i)) - \Phi_L(\xi_{\rm low}(\tau_i), \dot{\xi}_{\rm low}(\tau_i))\right). \quad (36)$$

Here, the sum extends over the time instances τ_i of all Bragg pulses transferring momenta along the two paths; see Fig. 1.

3. Atomic velocity after a photon interaction

Understanding how the Doppler effect and spacetime curvature affect the photon momentum transferred to the atoms undergoing Bragg transitions is necessary to calculate the boundary conditions of the atomic trajectories in Eq. (16). Note that calculating the momentum kicks bears a subtlety: the light field's momentum $\hbar k_\mu$ is a covector, whereas the atomic 4-velocity u^μ is a (contravariant) vector. Therefore, in order to compute the atomic velocity after the momentum kick, we need to raise the index of $\hbar k_\mu$ using the metric [81].

As an example, consider a Bragg pulse interacting with a wave packet at a height $z_{\rm int}$ as before. The additional velocity after the kick will then be given by

$$v_{\rm Kick} = \frac{\hbar}{m}\left(1 + 2\gamma\frac{g z_{\rm int}}{c^2}\right)k_R + \mathcal{O}(\Gamma c^{-2}). \quad (37)$$

4. Bloch oscillations: Accelerated optical lattices

For completeness, we also allow for accelerations of the atomic ensemble common to both IF arms using Bloch oscillations. In the experiment, the atoms are initially loaded into an optical lattice which is then accelerated. After unloading the atoms, they have gained an effective momentum, which we will denote by $\pm\hbar k_B$; the sign of the momentum transfer depends on whether momentum was gained in the positive or negative z direction. We adopt here a highly simplified description by assuming that Bloch oscillations only impart the desired momentum of $\pm\hbar k_B$, that the interaction is infinitely short—i.e., negligibly short compared to the timescale of the IF—and that the whole process is lossless. A microscopic description of the underlying physics [28,82] and its relativistic corrections are beyond the scope of the current article. Indeed, for the regime of large-momentum transfer [83,84], the theoretical description of Bloch oscillations is the subject of current investigations [85]. In analogy to the case of Bragg pulses treated before, we will denote the imprinted laser phase during one Bloch interaction as $\Phi_{L,B}(z) = \pm k_B z$, or written dimensionless, as $\Phi_{L,B}(\xi) = \pm\omega_{\rm C} T_R \mathcal{R}_{\rm B}\xi$. Hence, the relative Bloch laser phase can be written in terms of dimensionless quantities as

$$\Delta\Phi_{L,B} = \sum_i \Phi_{L,B}(\xi_{\rm up}(\tau_i)) - \Phi_{L,B}(\xi_{\rm low}(\tau_i)), \quad (38)$$

where the summation is taken over all interaction times τ_i that imprint a Bloch momentum.

IV. RESULTS

So far, we have calculated the three different kinds of phase shift contributions of an atom IF—namely, the propagation phase [Eq. (19)], the separation phase [Eq. (21)], and the laser phases [Eqs. (36) and (38) for, respectively, Bragg and Bloch pulses]—all of which include relativistic corrections up to the $\mathcal{O}(c^{-2})$ level. We are now in a position to determine the phase for a given IF geometry, pursuing a number of goals: (i) The phase is to be determined algebraically, similar to the results for the Mach-Zehnder IF in Dimopoulos *et al.* [32]. (ii) The algebraic expressions shall achieve correctness in $\mathcal{O}(c^{-2})$ and $\mathcal{O}(4)$ in the small parameters from Table I.

TABLE II. Complete list of phases of the SRBI, SDDI, and ARBI geometries in PPN spacetime written in terms of dimensionless parameters of order $\mathcal{O}(2)$ (rows #1–#3) and $\mathcal{O}(3)$ (rows #4–#24). To extract this phase for one of the IF geometries, multiply the factor in the column "Proportionality" by the time given in the column of the respective IF and the atomic Compton frequency ω_{C} in Eq. (20). For example, phase shift #1 for the SRBI is $\mathcal{R}_{\mathrm{R}}\mathcal{G}_{1,\mathrm{R}}\omega_{\mathrm{C}}(T_R+T_B)$, which translates into $gk_R(T_R^2+T_RT_B)$; see Table I. Written out in terms of dimensionful quantities, each contribution is a polynomial in T_R and T_B—i.e., it is proportional to $T_R^{\alpha_R}T_B^{\alpha_B}$. The overall exponent $\alpha=\alpha_R+\alpha_B$ determines the scaling of each phase with IF time.

			Phases in units of ω_{C}				
#	Order	Proportionality	Symmetric Ramsey-Bordé IF (SRBI)	Symmetric double diffraction IF (SDDI)	Asymmetric Ramsey-Bordé IF (ARBI)	α	Origin
1	$\mathcal{O}(2)$	$\mathcal{G}_{1,\mathrm{R}}\mathcal{R}_{\mathrm{R}}$	T_B+T_R	$2T_B+2T_R$	T_B+T_R	2	Nonrelativistic
2		$\mathcal{R}_{\mathrm{R}}^2$	0	0	T_R	1	
3		$\mathcal{R}_{\mathrm{R}}\mathcal{R}_{\mathrm{B}}$	$-T_R$	$-2T_R$	$-T_R$	1	
4	$\mathcal{O}(3)$	$\mathcal{R}_{\mathrm{R}}\mathcal{G}_0\mathcal{G}_{1,\mathrm{R}}$	$2(\beta-1)T_B+2(\beta-1)T_R$	$4(\beta-1)T_B+4(\beta-1)T_R$	$2(\beta-1)T_B+2(\beta-1)T_R$	2	PPN
5		$\mathcal{R}_{\mathrm{R}}\mathcal{Z}_0\mathcal{G}_{2,\mathrm{R}}$	$-T_B-T_R$	$-2T_B-2T_R$	$-T_B-T_R$	2	Gravity gradient
6		$\mathcal{R}_{\mathrm{R}}\mathcal{V}_0\mathcal{G}_{2,\mathrm{R}}$	$-\frac{3}{2}T_B-T_R$	$-3T_B-2T_R$	$-\frac{3}{2}T_B-T_R$	3	
7		$\mathcal{R}_{\mathrm{R}}\mathcal{R}_{\mathrm{B}}\mathcal{G}_{2,\mathrm{R}}$	$-\frac{1}{4}T_B-\frac{1}{6}T_R$	$-\frac{1}{2}T_B-\frac{1}{3}T_R$	$-\frac{1}{4}T_B-\frac{1}{6}T_R$	4	
8		$\mathcal{R}_{\mathrm{R}}\mathcal{G}_{1,\mathrm{R}}\mathcal{G}_{2,\mathrm{R}}$	$\frac{7}{6}T_B+\frac{7}{12}T_R$	$\frac{7}{3}T_B+\frac{7}{6}T_R$	$\frac{7}{6}T_B+\frac{7}{12}T_R$	4	
9		$\mathcal{R}_{\mathrm{R}}^2\mathcal{G}_{2,\mathrm{R}}$	$-\frac{1}{2}T_B-\frac{1}{2}T_R$	0	$-\frac{1}{2}T_B-\frac{1}{3}T_R$	3	
10		$\mathcal{R}_{\mathrm{R}}\mathcal{V}_0\mathcal{G}_{2,\mathrm{B}}$	$-\frac{1}{2}T_R$	$-T_R$	$-\frac{1}{2}T_R$	3	
11		$\mathcal{R}_{\mathrm{R}}\mathcal{R}_{\mathrm{B}}\mathcal{G}_{2,\mathrm{B}}$	$-\frac{1}{8}T_R$	$-\frac{1}{4}T_R$	$-\frac{1}{8}T_R$	3	
12		$\mathcal{R}_{\mathrm{R}}\mathcal{G}_{1,\mathrm{R}}\mathcal{G}_{2,\mathrm{B}}$	$\frac{1}{6}T_B+\frac{3}{4}T_R$	$\frac{1}{3}T_B+\frac{3}{2}T_R$	$\frac{1}{6}T_B+\frac{3}{4}T_R$	4	
13		$\mathcal{F}_{\mathrm{R}}\mathcal{G}_{1,\mathrm{R}}^2$	$-\frac{9}{2}T_B-3T_R$	$-9T_B-6T_R$	$-\frac{9}{2}T_B-3T_R$	3	Doppler effect
14		$\mathcal{F}_{\mathrm{R}}\mathcal{G}_{1,\mathrm{R}}\mathcal{V}_0$	$3T_B+3T_R$	$6T_B+6T_R$	$3T_B+3T_R$	2	
15		$\mathcal{F}_{\mathrm{R}}\mathcal{G}_{1,\mathrm{R}}\mathcal{G}_{1,\mathrm{B}}$	$-\frac{3}{2}T_B$	$-3T_B$	$-\frac{3}{2}T_B$	3	
16		$\mathcal{F}_{\mathrm{R}}\mathcal{R}_{\mathrm{B}}\mathcal{G}_{1,\mathrm{R}}$	$\frac{5}{2}T_B+\frac{7}{2}T_R$	$5T_B+7T_R$	$\frac{5}{2}T_B+\frac{7}{2}T_R$	2	
17		$\mathcal{F}_{\mathrm{R}}\mathcal{R}_{\mathrm{B}}^2$	$-T_R$	$-2T_R$	$-T_R$	1	
18		$\mathcal{F}_{\mathrm{R}}\mathcal{R}_{\mathrm{B}}\mathcal{V}_0$	$-2T_R$	$-4T_R$	$-2T_R$	1	
19		$\mathcal{F}_{\mathrm{R}}\mathcal{R}_{\mathrm{R}}^2$	0	$2T_R$	T_R	1	
20		$\mathcal{F}_{\mathrm{R}}\mathcal{R}_{\mathrm{R}}\mathcal{G}_{1,\mathrm{B}}$	$\frac{1}{2}T_B$	0	$-\frac{1}{2}T_B$	2	
21		$\mathcal{F}_{\mathrm{R}}\mathcal{R}_{\mathrm{R}}\mathcal{G}_{1,\mathrm{R}}$	$3T_B+\frac{5}{2}T_R$	0	$-3T_B-\frac{9}{2}T_R$	2	
22		$\mathcal{F}_{\mathrm{R}}\mathcal{R}_{\mathrm{R}}\mathcal{R}_{\mathrm{B}}$	$-\frac{1}{2}T_B-2T_R$	0	$\frac{1}{2}T_B+2T_R$	1	
23		$\mathcal{F}_{\mathrm{R}}\mathcal{R}_{\mathrm{R}}\mathcal{V}_0$	$-T_B-T_R$	0	T_B+5T_R	1	
24		$\mathcal{F}_{\mathrm{R}}\mathcal{R}_{\mathrm{R}}\mathcal{Z}_0$	0	0	$2T_R$	1	

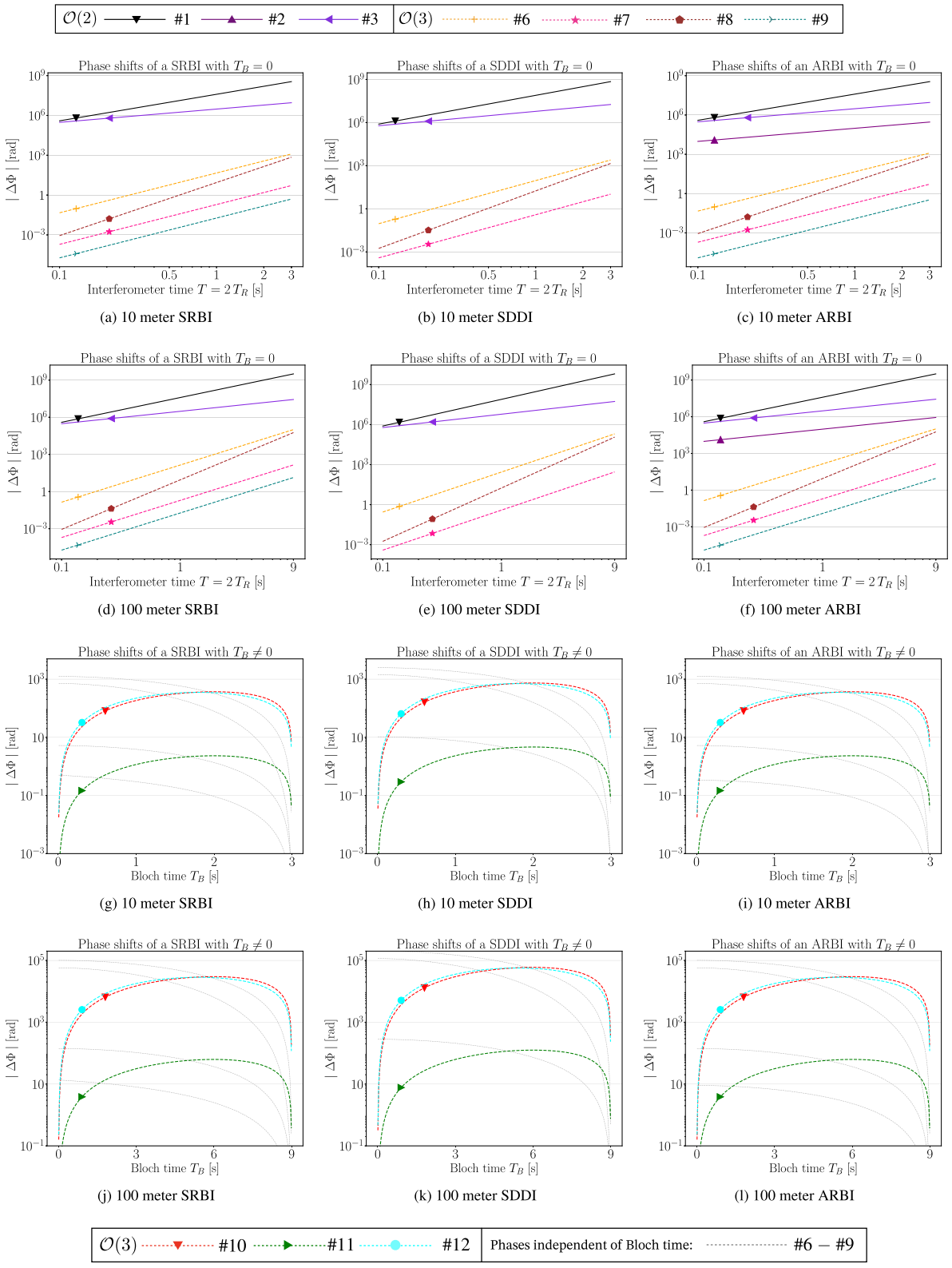

(a) 10 meter SRBI (b) 10 meter SDDI (c) 10 meter ARBI

(d) 100 meter SRBI (e) 100 meter SDDI (f) 100 meter ARBI

(g) 10 meter SRBI (h) 10 meter SDDI (i) 10 meter ARBI

(j) 100 meter SRBI (k) 100 meter SDDI (l) 100 meter ARBI

FIG. 2. Phase shift contributions in the three IF geometries SRBI, SDDI, and ARBI for 10 m and 100 m baselines. Solid curves correspond to phase shifts of order $\mathcal{O}(2)$ and dashed curves to $\mathcal{O}(3)$ shifts. (a)–(f) The Bloch time T_B is set to zero, and all nonzero phase shift contributions are plotted with respect to time $T = 2T_R$. (f)–(l) Colored phase shift contributions depend nontrivially on T_B and are plotted against T_B for a fixed time $T = 2T_R + T_B$ of 3 seconds (9 seconds) for the 10 m (100 m) baseline; the gray curves correspond to the Bloch-time-independent phase contributions from (a)–(f). In addition to the numerical values in Table I, the plots assume numerical values of $g = 9.81\ \mathrm{ms}^{-2}$ and $\Gamma = 1.54 \times 10^{-6}\ \mathrm{s}^{-2}$.

(iii) The routine for calculating the phase should be applicable to a general class of IFs consisting of arbitrary sequences of Bragg and Bloch pulses.

We consider IFs characterized by (a) a list of n time intervals of free propagation between light pulses and (b) two lists of $n+1$ momenta transferred by Bragg or Bloch pulses in the upper and lower IF paths; see Eq. (16). For an IF geometry defined by these lists, first the classical trajectories—and from these the propagation, separation, and laser phases—must be calculated to the desired accuracy $\mathcal{O}(c^{-2})$ and $\mathcal{O}(4)$. The required algebra is rather tedious and error prone and therefore relegated entirely to computer algebra based on Python; see [33]. The code exploits the fact that the required arithmetics and integrals can be mapped onto list manipulations for keeping track of the small dimensionless parameters in Table I.

In the following, we will discuss the results for the three specific IF geometries shown in Fig. 1, which we refer to as the symmetric Ramsey-Bordé interferometer (SRBI), symmetric double diffraction interferometer (SDDI), and asymmetric Ramsey-Bordé interferometer (ARBI). In Table II, we present the main result of this analysis—i.e., a list of phase shifts of the SRBI, ARBI, and SDDI geometries from Figs. 1(a)–1(c) where we display all terms of orders $\mathcal{O}(2)$ and $\mathcal{O}(3)$. The higher-order terms of $\mathcal{O}(4)$ are too numerous to be listed, but they can be explicitly obtained from [33].

The three $\mathcal{O}(2)$ terms are the well-known nonrelativistic phases due to linearized gravity and Bragg as well as Bloch recoils; see rows #1 – #3 in Table II. The 21 $\mathcal{O}(3)$ terms can be grouped as arising from three main sources: (i) The first is caused by PPN terms which result from nonlinear gravitational effects, as indicated by their dependence on $\mathcal{G}_0$. (ii) The second arises by the gravity gradient, as one can infer from their dependence on $\mathcal{G}_{2,\mathrm{R}}$ or $\mathcal{G}_{2,\mathrm{B}}$. (iii) The third stems from the Doppler effect, as is evident from the dependence on $\mathcal{F}_{\mathrm{R}}$. Other $\mathcal{O}(c^{-2})$ or Λ-dependent phase shifts naturally appear at the $\mathcal{O}(4)$ level. Comparing the phases for the three IF geometries, one can see that most of the terms are identical in the SRBI and ARBI, and differ from the SDDI by a factor of 2. This is due to the fact that the enclosed spacetime area in the SDDI is twice as big as in the other two IFs. Connections between the enclosed spacetime area and the IF phases were analyzed in detail by [86]. Terms like #2 and #9, however, differ quite significantly between the different IF geometries. The first of those terms was described in [16] via a special relativistic proper time difference, whereas the latter was phrased as a "first gradient recoil" effect in [32] and was explained in Appendix F of [19]. Phases #19 – #24, which relate to the Doppler effect due to the transferred Bragg momentum $\mathcal{R}_{\mathrm{R}}$, also differ between the IF geometries in a nontrivial manner. The phases linear in $\mathcal{R}_{\mathrm{R}}$ cancel in the SDDI due to its symmetry, but they are nonzero in the ARBI and the SRBI.

In Fig. 2, we plot the phase shifts of $\mathcal{O}(2)$ and the leading contributions of $\mathcal{O}(3)$ evaluated for two case studies, corresponding to a 10 m and a 100 m baseline IF. The resulting list of phase shifts can be grouped into two categories: Figs. 2(a)–2(f) show phases that are maximal for $T_B = 0$ and therefore would preferably be analyzed in an IF without Bloch pulses (vanishing Bloch time T_B). Figures 2(g)–2(l) display phases that are functions of the Bloch recoil and therefore are maximal for a nontrivial combination of T_R and T_B, since the corresponding phase shift will vanish in both limiting cases—i.e., $T_B = 0$ and $T_R = 0$. It can be observed that the curves of $\mathcal{O}(2)$ and $\mathcal{O}(3)$ cluster with a gap of several orders of magnitude between them. The magnitude of the $\mathcal{O}(4)$ terms will be smaller by about the same factor—i.e., those terms contribute around 10^{-10} rad for short IF times of around 0.1 seconds. The Doppler-related $\mathcal{O}(3)$ terms will, however, also be present at $\mathcal{O}(4)$, because of the comparably small value of ω_R and therefore $\mathcal{F}_{\mathrm{R}}$; see Table I.

For the specific case of a Mach-Zehnder IF (equivalent to the SRBI with $k_B = 0, T_B = 0$), we can compare the results of our treatment to that of Dimopoulos *et al.* [31,32] and find good, although not exact, agreement. A detailed comparison of the terms up to $\mathcal{O}(4)$ can be found in Appendix E, in which we also summarize where our approach differs from that of [31,32] in methodology and notation and discuss how these differences affect the final results.

V. DISCUSSION AND SUMMARY

Starting from a post-Newtonian approximation of the Schrödinger equation in a curved spacetime, described by a metric theory of gravity, we have presented a calculation of the phase contributions of a whole class of light-pulse atom IFs. The phases are derived from a relativistically corrected, quantum-optical Hamiltonian for atoms and light in a PPN spacetime, written in a locally orthonormal coordinate system and applied to the specific case of atom IFs that use elastic scattering processes. After following the standard procedure for calculating phases in atom IFs in the presence of relativistic corrections, we have expressed all the resulting phase contributions as functions of dimensionless parameters that arise naturally from this description. The computation of all phase contributions up to a desired order in those dimensionless parameters for any IF geometry consisting of Bragg and Bloch pulses is automated in Python. We have illustrated the results of this algorithm using three exemplary IF geometries and compared their individual phase contributions algebraically and, for the dominant contributions, quantitatively for long-baseline IFs. With a suitable choice of IF geometries, it may then be possible to find new measurement strategies for differential IF setups, which particularly enhance individual phase contributions and suppress terms which are of minor interest.

This analysis can be extended to IFs that use inelastic scattering processes—e.g., Raman transitions [19,29,69,87]—and would also be sufficient to describe stationary spacetimes, which could include effects of Earth's rotation and describe gravitomagnetic phenomena such as the Lense-Thirring effect [78]. One would then, however, need to include all FSL effects, since instantaneous laser pulses would require the notion of simultaneity, which is not necessarily well defined in nonstatic spacetimes. The description of spaceborne experiments could also be a natural extension of this formalism, in which one would need to go beyond our approximation of the gravitational potential, due to possibly elliptical orbits with a considerable height variation. Another interesting approach one could pursue is to start from a Hamiltonian that describes fermionic particles in curved spacetime, cf. [88], and investigate whether spin-related interactions with gravity might give rise to interesting tests of GR in light-pulse atom IFs.

ACKNOWLEDGMENTS

Funded by the Deutsche Forschungsgemeinschaft (DFG)—SFB 1227, DQ-mat'—Project-ID No. 274200144, project A05. We thank Ernst Rasel, Dennis Schlippert, Christian Schubert, and Enno Giese for insightful discussions.

APPENDIX A: TRANSFORMATION INTO NEW COORDINATES

We want to construct a coordinate transformation $(\mathsf{x}^\mu) = (c\mathsf{t}, \mathbf{r}) \mapsto (x^\mu) = (ct, \boldsymbol{r})$ that brings the metric tensor to Minkowskian form at the point of the experiment, which in this appendix we will generically denote by p_0 (in the main text, this is taken as a point on the surface of the Earth). Since the asymptotic coordinates in which the metric was originally expressed in Eq. (1) are already orthogonal to our order of approximation, in order to bring the metric to Minkowskian form at p_0, we only have to perform a coordinate transformation such as to normalize the new coordinate basis vectors at this point. This can most easily be realized by globally rescaling the coordinates by the corresponding (constant) normalization factor: defining the new coordinates according to

$$x^\mu = \sqrt{|\mathsf{g}_{\mu\mu}(p_0))|}\,\mathsf{x}^\mu \tag{A1}$$

(no summation over μ), the new coordinate basis vectors are given by

$$\frac{\partial}{\partial x^\mu} = \frac{1}{\sqrt{|\mathsf{g}_{\mu\mu}(p_0))|}}\frac{\partial}{\partial \mathsf{x}^\mu}, \tag{A2}$$

which are normalized at p_0.

Explicitly, defining $\phi_0 = \phi(p_0)$, the metric length of the timelike coordinate basis vector $\frac{\partial}{\partial \mathsf{x}^0}|_{p_0} = \frac{1}{c}\frac{\partial}{\partial \mathsf{t}}|_{p_0}$ of the asymptotic (i.e., old) coordinates is given by

$$\begin{aligned}\sqrt{-\mathsf{g}_{00}(p_0)} &= \sqrt{1 + 2\frac{\phi_0}{c^2} + 2\beta\frac{\phi_0^2}{c^4} + \mathcal{O}(c^{-6})} \\ &= 1 + \frac{\phi_0}{c^2} + \frac{2\beta - 1}{2}\frac{\phi_0^2}{c^4} + \mathcal{O}(c^{-6}),\end{aligned} \tag{A3a}$$

while the metric length of the spacelike coordinate basis vector $\frac{\partial}{\partial \mathsf{x}^i}|_{p_0}$ of the asymptotic coordinates is (without summation over i)

$$\begin{aligned}\sqrt{\mathsf{g}_{ii}(p_0)} &= \sqrt{1 - 2\gamma\frac{\phi_0}{c^2} + \mathcal{O}(c^{-4})} \\ &= 1 - \gamma\frac{\phi_0}{c^2} + \mathcal{O}(c^{-4}).\end{aligned} \tag{A3b}$$

Therefore, we may take the constantly rescaled new coordinates expressed in terms of the old coordinates as

$$t = \left(1 + \frac{\phi_0}{c^2} + \frac{2\beta - 1}{2}\frac{\phi_0^2}{c^4}\right)\mathsf{t}, \tag{A4a}$$

$$\boldsymbol{r} = \left(1 - \gamma\frac{\phi_0}{c^2}\right)\mathbf{r}. \tag{A4b}$$

The inverse transformation is then given by

$$\mathsf{t} = \left(1 - \frac{\phi_0}{c^2} - \frac{2\beta - 3}{2}\frac{\phi_0^2}{c^4} + \mathcal{O}(c^{-6})\right)t, \tag{A5a}$$

$$\mathbf{r} = \left(1 + \gamma\frac{\phi_0}{c^2} + \mathcal{O}(c^{-4})\right)\boldsymbol{r}. \tag{A5b}$$

Now, computing the components of the metric in the new coordinates according to

$$g_{\mu\nu} = \frac{\partial \mathsf{x}^\lambda}{\partial x^\mu}\frac{\partial \mathsf{x}^\sigma}{\partial x^\nu}\mathsf{g}_{\lambda\sigma}, \tag{A6}$$

we obtain the new spatial components

$$g_{ij}(\boldsymbol{r}) = \left(1 - 2\gamma\frac{\bar{\phi}(\boldsymbol{r})}{c^2}\right)\delta_{ij} + \mathcal{O}(c^{-4}) \tag{A7}$$

and the new temporal component

$$\begin{aligned}g_{00}(\boldsymbol{r}) = -1 &- 2\frac{\bar{\phi}(\boldsymbol{r})}{c^2} - 2\beta\frac{\bar{\phi}(\boldsymbol{r})^2}{c^4} \\ &- 4(\beta - 1)\phi_0\frac{\bar{\phi}(\boldsymbol{r})}{c^4} + \mathcal{O}(c^{-6}),\end{aligned} \tag{A8}$$

where we use the definition of a shifted gravitational potential—i.e., $\bar{\phi}(\boldsymbol{r}) = \phi(\boldsymbol{r}) - \phi_0$.

The line element in the new coordinates reads

$$\mathrm{d}s^2 = -\left(c^2 + 2\bar{\phi} + 2\beta\frac{\bar{\phi}^2}{c^2} + 4(\beta-1)\frac{\phi_0\bar{\phi}}{c^2}\right)\mathrm{d}t^2 + \left(1 - 2\gamma\frac{\bar{\phi}}{c^2}\right)\mathrm{d}\boldsymbol{r}^2 + \mathcal{O}(c^{-4}), \tag{A9}$$

which is Minkowskian at the reference point. The components of the inverse metric are then

$$g^{\mu\nu}(\boldsymbol{r}) = \begin{pmatrix} -1 + 2\frac{\bar{\phi}(\boldsymbol{r})}{c^2} + (2\beta-4)\frac{\bar{\phi}(\boldsymbol{r})^2}{c^4} + 4(\beta-1)\phi_0\frac{\bar{\phi}(\boldsymbol{r})}{c^4} + \mathcal{O}(c^{-6}) & \mathcal{O}(c^{-5}) \\ \mathcal{O}(c^{-5}) & \left(1 + 2\gamma\frac{\bar{\phi}(\boldsymbol{r})}{c^2}\right)\mathbb{I}_3 + \mathcal{O}(c^{-4}) \end{pmatrix}, \tag{A10}$$

where $\mathbb{I}_3$ is the 3×3 identity matrix. Using these expressions, we can calculate the Christoffel symbols $\Gamma^{\mu}{}_{\nu\sigma} = \frac{1}{2}g^{\mu\lambda}(g_{\lambda\nu,\sigma} + g_{\lambda\sigma,\nu} - g_{\nu\sigma,\lambda})$. We assume that the Newtonian gravitational potential is time independent—i.e., $\partial_t\phi = 0$. The trivial Christoffel symbols are $\Gamma^0{}_{00} = \mathcal{O}(c^{-7})$, $\Gamma^0{}_{ij} = \mathcal{O}(c^{-5})$, and $\Gamma^i{}_{j0} = \mathcal{O}(c^{-5})$, whereas the nonvanishing Christoffel symbols are

$$\Gamma^0{}_{i0} = \Gamma^0{}_{0i} = \left(1 + 2(\beta-1)\frac{\phi}{c^2}\right)\frac{\bar{\phi}_{,i}}{c^2} + \mathcal{O}(c^{-6}), \tag{A11a}$$

$$\Gamma^i{}_{00} = \left(1 + 2(\beta+\gamma)\frac{\phi}{c^2} - 2(\gamma+1)\frac{\phi_0}{c^2}\right)\frac{\delta^{ij}\bar{\phi}_{,j}}{c^2} + \mathcal{O}(c^{-6}), \tag{A11b}$$

$$\Gamma^i{}_{jk} = -\gamma\frac{\delta^i{}_j\bar{\phi}_{,k} + \delta^i{}_k\bar{\phi}_{,j} - \delta_{jk}\delta^{il}\bar{\phi}_{,l}}{c^2} + \mathcal{O}(c^{-4}). \tag{A11c}$$

APPENDIX B: EULER-LAGRANGE EQUATION AND PROPAGATION PHASE

The motional relativistic Lagrangian corresponding to a point particle with mass m in a spacetime with a metric tensor $g_{\mu\nu}$ can be obtained via $L_\mathrm{M} = -mc\sqrt{-g_{\mu\nu}\frac{\mathrm{d}x^\mu}{\mathrm{d}t}\frac{\mathrm{d}x^\nu}{\mathrm{d}t}}$. This evaluates for a trajectory in the z direction to

$$L_\mathrm{M} = -mc^2 + \frac{m\dot{z}(t)^2}{2} - m\bar{\phi}(z(t)) + \frac{m\dot{z}(t)^4}{8c^2} - m\frac{2\beta-1}{2}\frac{\bar{\phi}(z(t))^2}{c^2} - m\frac{2\gamma+1}{2}\frac{\bar{\phi}(z(t))\dot{z}(t)^2}{c^2} - 2(\beta-1)m\phi_0\frac{\bar{\phi}(z(t))}{c^2} + \mathcal{O}(c^{-4}). \tag{B1}$$

From this, we can deduce the Euler-Lagrange equation. We first calculate the derivatives as

$$\frac{\partial L_\mathrm{M}}{\partial z} = -m\partial_z\bar{\phi}(z) + \frac{m}{c^2}\left[-(2\beta-1)\bar{\phi}(z)\partial_z\bar{\phi}(z) - \frac{2\gamma+1}{2}\dot{z}^2\partial_z\bar{\phi}(z) - 2(\beta-1)\phi_0\partial_z\bar{\phi}(z)\right] + \mathcal{O}(c^{-4}), \tag{B2a}$$

$$\frac{\partial L_\mathrm{M}}{\partial \dot{z}} = m\dot{z} + \frac{m}{c^2}\left[\frac{1}{2}\dot{z}^3 - (2\gamma+1)\bar{\phi}(z)\dot{z}\right] + \mathcal{O}(c^{-4}), \tag{B2b}$$

$$\frac{\mathrm{d}}{\mathrm{d}t}\frac{\partial L_\mathrm{M}}{\partial \dot{z}} = m\ddot{z} + \frac{m}{c^2}\left[\frac{3}{2}\dot{z}^2\ddot{z} - (2\gamma+1)\dot{z}^2\partial_z\bar{\phi}(z) - (2\gamma+1)\bar{\phi}(z)\ddot{z}\right] + \mathcal{O}(c^{-4}), \tag{B2c}$$

where we have used the fact that $\dot{\bar{\phi}}(z)\dot{z} = \dot{z}^2\partial_z\bar{\phi}(z)$, which holds because $\frac{\mathrm{d}}{\mathrm{d}t}\bar{\phi}(z(t)) = \frac{\partial\bar{\phi}}{\partial z}\frac{\mathrm{d}z}{\mathrm{d}t}$. The Euler-Lagrange equation $\frac{\mathrm{d}}{\mathrm{d}t}\frac{\partial L_\mathrm{M}}{\partial\dot{z}} - \frac{\partial L_\mathrm{M}}{\partial z} = 0$ can then be written recursively in terms of $\ddot{z}$ as

$$\ddot{z} = -\partial_z\bar{\phi}(z) + \frac{1}{c^2}\left[(2\gamma+1)\dot{z}^2\partial_z\bar{\phi}(z) - \frac{3}{2}\dot{z}^2\ddot{z} + (2\gamma+1)\bar{\phi}(z)\ddot{z} - (2\beta-1)\bar{\phi}(z)\partial_z\bar{\phi}(z) - \frac{2\gamma+1}{2}\dot{z}^2\partial_z\bar{\phi}(z) - 2(\beta-1)\phi_0\partial_z\bar{\phi}(z)\right] + \mathcal{O}(c^{-4}).$$

Inserting the c^0 contribution into the $\ddot{z}$ term on the right-hand side results in

$$\ddot{z} = -\partial_z\left[\left(1+2(\beta-1)\frac{\phi_0}{c^2}\right)\bar{\phi}(z)+\frac{\beta+\gamma}{c^2}\bar{\phi}(z)^2\right] + \frac{\gamma+2}{c^2}\dot{z}^2\partial_z\bar{\phi}(z)+\mathcal{O}(c^{-4}). \tag{B3}$$

We now use the approximation of the gravitational potential to relevant order—i.e., $\bar{\phi}(z)=gz-\frac{1}{2}\Gamma z^2+\frac{1}{3}\Lambda z^3+\mathcal{O}(\partial_r^4\phi)$—which gives the Euler-Lagrange equation

$$\begin{aligned}\ddot{z}(t) = &-\left(1+2(\beta-1)\frac{\phi_0}{c^2}\right)g+\left(1+2(\beta-1)\frac{\phi_0}{c^2}\right)\Gamma z(t)\\ &-\Lambda z(t)^2-2g^2\frac{\beta+\gamma}{c^2}z(t)+(\gamma+2)\frac{g}{c^2}\dot{z}(t)^2\\ &+\mathcal{O}(\partial_r^4\phi,\Lambda c^{-2},c^{-4}),\end{aligned} \tag{B4}$$

with initial conditions $z(0)=z_0$, $\dot{z}(0)=v_0+N_R\frac{\hbar k_R}{m}+N_B\frac{\hbar k_B}{m}$, which in the main text was written using the dimensionless trajectory $\xi(\tau)$ as

$$\begin{aligned}\ddot{z}(\tau) = &-\mathcal{G}_{1,\mathrm{R}}+\mathcal{G}_{2,\mathrm{R}}\xi(\tau)-\mathcal{G}_{3,\mathrm{R}}\xi(\tau)^2-2(\beta+\gamma)\mathcal{G}_{1,\mathrm{R}}^2\xi(\tau)\\ &+(\gamma+2)\mathcal{G}_{1,\mathrm{R}}\dot{\xi}(\tau)^2+2(\beta-1)\mathcal{G}_0[-\mathcal{G}_{1,\mathrm{R}}+\mathcal{G}_{2,\mathrm{R}}\xi(\tau)]\\ &+\mathcal{O}(4),\end{aligned} \tag{B5}$$

with initial conditions $\xi(0)=\mathcal{Z}_0$, $\dot{\xi}(0)=\mathcal{V}_0+N_R\mathcal{R}_\mathrm{R}+N_B\mathcal{R}_\mathrm{B}$. The perturbative solution of this equation to second order reads

$$\begin{aligned}\xi(\tau) = &\xi(0)+\dot{\xi}(0)\tau-\frac{1}{2}(1+2(\beta-1)\mathcal{G}_0)\mathcal{G}_{1,\mathrm{R}}\tau^2\\ &+\mathcal{G}_{2,\mathrm{R}}\left(\frac{1}{2}\xi(0)\tau^2+\frac{1}{6}\dot{\xi}(0)\tau^3-\frac{1}{24}\mathcal{G}_{1,\mathrm{R}}\mathcal{G}_{2,\mathrm{R}}\tau^4\right)\\ &+\mathcal{O}(3).\end{aligned} \tag{B6}$$

The propagation phase is given by the time integral over $L_\mathrm{M}/\hbar$, which we can now translate into dimensionless quantities as explained in the main text. We obtain

$$\begin{aligned}\frac{1}{\hbar}\int L_\mathrm{M}\mathrm{d}t = \omega_\mathrm{C}T_R\int\Big(&-\mathcal{G}_{1,\mathrm{R}}\xi(\tau)+\frac{1}{2}\mathcal{G}_{2,\mathrm{R}}\xi(\tau)^2-\frac{1}{3}\mathcal{G}_{3,\mathrm{R}}\xi(\tau)^3+\frac{1}{2}\dot{\xi}(\tau)^2+\frac{1}{8}\dot{\xi}(\tau)^4-\frac{2\beta-1}{2}\mathcal{G}_{1,\mathrm{R}}^2\xi(\tau)\\ &-\frac{2\gamma+1}{2}\mathcal{G}_{1,\mathrm{R}}\xi(\tau)\dot{\xi}(\tau)^2-2(\beta-1)\mathcal{G}_0\mathcal{G}_{1,\mathrm{R}}\xi(\tau)+2(\beta-1)\mathcal{G}_0\mathcal{G}_{2,\mathrm{R}}\xi(\tau)^2\Big)\mathrm{d}\tau+\mathcal{O}(5).\end{aligned} \tag{B7}$$

APPENDIX C: MAXWELL'S EQUATIONS IN CURVED SPACETIME

Let us start again with Maxwell's equations in vacuum—i.e.,

$$F^{\alpha\beta}{}_{;\beta}=\nabla_\beta F^{\alpha\beta}=\nabla_\beta(\nabla^\alpha A^\beta-\nabla^\beta A^\alpha)=0, \tag{C1}$$

where we have expressed the field strength tensor in terms of the (4-)vector potential A^α. Commuting the covariant derivatives in the first term at the expense of introducing a curvature term, this becomes

$$A^\beta{}_{;\beta}{}^{;\alpha}+R^\alpha{}_\beta A^\beta-A^{\alpha;\beta}{}_{;\beta}=0. \tag{C2}$$

From now on, working in the Lorenz gauge with gauge condition

$$A^\beta{}_{;\beta}=0, \tag{C3a}$$

this simplifies to

$$-A^{\alpha;\beta}{}_{;\beta}+R^\alpha{}_\beta A^\beta=0. \tag{C3b}$$

(We will later comment on how the Lorenz gauge is in our case related to the Coulomb gauge, which is the one that is commonly employed in quantum optics.)

1. Geometric optics approximation

We now want to solve these equations in the approximation of geometric optics, which, following [[89], §22.5], we implement by a series expansion. This approach was also recently used in [90] to describe the light propagation in atom IFs with a nonvanishing dilaton field. Denoting the wavelength of the light field by λ, we can deduce the two important length scales for the approximation to be

$$\begin{aligned}\mathcal{R} &= \left|\begin{array}{c}\text{typical component of } R^\mu{}_{\nu\sigma\tau} \text{ as}\\ \text{measured in a local Lorentz frame}\end{array}\right|^{-\frac{1}{2}}\\ &\approx \left|\partial_r\frac{\bar{\phi}}{c^2}\right|^{-\frac{1}{2}}\approx 10^8\ \mathrm{m}\\ \mathcal{L} &= \left|\begin{array}{c}\text{radius of curvature}\\ \text{of a wave front}\end{array}\right|\approx 1\ \mathrm{mm}.\end{aligned}$$

We then define the small expansion parameter

$$\epsilon=\lambda/(2\pi\min(\mathcal{R},\mathcal{L}))=\lambda/(2\pi\mathcal{L}),$$

which can be thought of as the ratio of the wavelength of the light field to the length scale $\mathcal{L}$ of the variation of a slowly varying envelope of the field, divided by 2π. We now assume the 4-potential to be given by

$$A_\mu = (a_\mu + \mathcal{O}(\epsilon))e^{\mathrm{i}\Phi/\epsilon}, \tag{C4}$$

where the components $a_\mu\colon \mathcal{M} \to \mathbb{C}$ of the leading-order amplitude are complex-valued functions on spacetime, and $\Phi\colon \mathcal{M} \to \mathbb{R}$ is the real-valued phase. The relativistic wave vector (or 4-wave-vector) is then defined as $k = \mathrm{d}\Phi$—i.e., in components $k_\mu = \partial_\mu \Phi$. Following [[89], §22.5], we will refer to everything of order up to ϵ^{-1} as "geometric optics," whereas we will ignore "postgeometric optics" orders—i.e., orders ϵ^0 and higher.

Plugging the ansatz [Eq. (C4)] into Maxwell's equations [Eq. (C3b)] and the Lorenz gauge condition [Eq. (C3a)] and grouping terms by their orders in ϵ, one obtains the following (for derivations, see [89], §22.5):

(1) Equation (C3b) at leading order ϵ^{-2} is equivalent to the wave vector k_μ being lightlike—i.e., satisfying $k_\mu k^\mu = g^{\mu\lambda}k_\mu k_\lambda = 0$. Taking the covariant derivative of this condition and using the fact that $k = \mathrm{d}\Phi$, one further obtains that k_μ must be geodesic—i.e., it must satisfy $k^\mu \nabla_\mu k^\nu = 0$.

(2) Equation (C3a) at leading order ϵ^{-1} is equivalent to $k^\mu a_\mu = 0$—i.e., the leading-order amplitude is orthogonal to the wave vector.

(3) Equation (C3b) at subleading order ϵ^{-1} determines the propagation law for a_μ along the "light rays" (i.e., null geodesics integrating the vector field k^μ): it must satisfy $k^\mu \nabla_\mu a_\nu = -\frac{1}{2} a_\nu \nabla_\mu k^\mu$. Note that combining this propagation law with the geodesic equation for k^μ implies $k^\mu \nabla_\mu (a_\nu k^\nu) = -\frac{1}{2}(\nabla_\mu k^\mu)(a_\nu k^\nu)$, such that if we start integrating the propagation law along a geodesic with an initial a_μ that is orthogonal to k^μ, this will automatically continue to hold along the geodesic.

a. Calculating the wave vector

Because we have assumed our spacetime to be stationary with a timelike Killing vector field $\partial_0 = c^{-1}\partial_t$, we know that, to the level of approximation we are working with, the wave vector's corresponding timelike component $k_0 = k_\mu (\partial_0)^\mu = c^{-1}\partial_t \Phi$ is constant along each geodesic/light ray that arises as an integral curve of the vector field k^μ. Note that due to the normalization of the phase in the ansatz Eq. (C4), differently from the main text, the light's angular frequency as measured by a stationary observer at rest at the experiment's reference point is now given by $\omega_0 = -ck_0/\epsilon$. We will keep this normalization for the remainder of this appendix. Also, since all the remaining equations that we will be considering are linear in k_μ, the overall normalization of k_μ does not matter, and for notational convenience, we will treat it to be of order c^0 for the remainder of this appendix.

We will only consider EM waves traveling in one spatial dimension—namely, the z (i.e., vertical) direction. Therefore, we will take $k_x = k_y = 0$ and neglect the x and y dependence of k_μ. The condition of k^μ being lightlike then takes the form $0 = g^{\mu\lambda}k_\mu k_\lambda = (-1 + 2\frac{\bar{\phi}(z)}{c^2})k_0^2 + (1 + 2\gamma\frac{\bar{\phi}(z)}{c^2})k_z^2 + \mathcal{O}(c^{-4})$, or equivalently $k_z^2 = (1 - 2(\gamma+1)\frac{\bar{\phi}(z)}{c^2})k_0^2 + \mathcal{O}(c^{-4})$. We now also restrict our consideration to the case of neighboring "light rays" (i.e., null geodesics integrating the vector field k^μ) having the same timelike wave vector component k_0, such that for our purposes k_0 is constant. Therefore, to our order of approximation, the wave vector's z component is determined as

$$k_z = k_z(z) = \pm\left(1 - (\gamma+1)\frac{\bar{\phi}(z)}{c^2}\right)k_0 + \mathcal{O}(c^{-4}), \tag{C5}$$

with the sign depending on the direction of propagation. Hence, restricting to the (ct, z) components, we obtain the relativistic wave vector

$$(k_\mu(z)) = \begin{pmatrix} 1 \\ \pm\left(1 - (\gamma+1)\frac{\bar{\phi}(z)}{c^2}\right) \end{pmatrix} k_0 + \mathcal{O}(c^{-4}). \tag{C6}$$

Since $k_\mu = \Phi_{,\mu}$ we therefore know that the phase of the EM field is, to our order of approximation, given by

$$\Phi(z,t) = \Phi_0 + k_0 ct \pm \left(1 - \frac{\gamma+1}{2}\frac{gz}{c^2}\right)k_0 z + \mathcal{O}(\Gamma c^{-2}), \tag{C7}$$

where Φ_0 is an arbitrary offset, which we will set to zero. The contravariant components $k^\mu = g^{\mu\nu}k_\nu$ of the wave vector, which we will need below, are given by

$$(k^\mu(z)) = \begin{pmatrix} -1 + 2\frac{\bar{\phi}(z)}{c^2} \\ \pm\left(1 + (\gamma-1)\frac{\bar{\phi}(z)}{c^2}\right) \end{pmatrix} k_0 + \mathcal{O}(c^{-4}). \tag{C8}$$

b. Calculating the amplitude

We are now going to determine the leading-order amplitude a_μ by integrating its propagation law

$$k^\mu \nabla_\mu a_\nu = -\frac{1}{2} a_\nu \nabla_\mu k^\mu \tag{C9}$$

along the light rays/lightlike geodesics integrating k^μ. Considering the amplitude $a_\nu(s)$ along a single such

geodesic, with s denoting the affine parameter measured from $z = 0$, the propagation law takes the form

$$a_\nu'(s) = k^\mu \Gamma^\lambda_{\mu\nu} a_\lambda(s) - \frac{1}{2} a_\nu(s)(\nabla_\mu k^\mu), \tag{C10}$$

where the prime denotes a derivative with respect to s, and k^μ, the Christoffel symbols, and $\nabla_\mu k^\mu$ are of course also to be evaluated along the geodesic.

The divergence of k^μ evaluates to

$$\begin{aligned}\nabla_\mu k^\mu &= \partial_\mu k^\mu + k^\mu \Gamma^\rho_{\mu\rho} \\ &= \partial_\mu k^\mu + k^\mu \partial_\mu \ln\sqrt{-g} \\ &= \mp 2\gamma \frac{g}{c^2} k_0 + \mathcal{O}(\Gamma c^{-2}),\end{aligned} \tag{C11}$$

which follows from the explicit form of k^μ in Eq. (C8) and $\ln\sqrt{-g} = \ln\sqrt{1 + (2-6\gamma)\frac{\bar\phi}{c^2} + \mathcal{O}(c^{-4})} = (1-3\gamma)\frac{\bar\phi}{c^2} + \mathcal{O}(c^{-4})$. Inserting this and the explicit form of the Christoffel symbols, the amplitude propagation law Eq. (C10) takes the explicit form

$$a_0'(s) = \left(\pm(\gamma+1)\frac{g}{c^2} a_0(s) - \frac{g}{c^2} a_z(s)\right) k_0 + \mathcal{O}(\Gamma c^{-2}), \tag{C12a}$$

$$a_x'(s) = \mathcal{O}(\Gamma c^{-2}), \tag{C12b}$$

$$a_y'(s) = \mathcal{O}(\Gamma c^{-2}), \tag{C12c}$$

$$a_z'(s) = -\frac{g}{c^2} a_0(s) k_0 + \mathcal{O}(\Gamma c^{-2}). \tag{C12d}$$

To solve this first-order system of ODEs, we need an initial condition for the amplitude a_μ. We want this initial value $a_\mu(s=0)$ (i.e., the value at the point of the light ray at height $z = 0$) to be purely transversal—i.e., given by $(a_0(0), a_x(0), a_y(0), a_z(0)) = (0, \mathcal{A}_x, \mathcal{A}_y, 0)$. Note that this initial value is consistent with the condition $a_\mu k^\mu = 0$. We directly see that up to our level of approximation, the solution of Eq. (C12) with this initial condition is constant—i.e., we have

$$(a_0, a_x, a_y, a_z) = (0, \mathcal{A}_x, \mathcal{A}_y, 0) + \mathcal{O}(\Gamma c^{-2}) \tag{C13}$$

along the whole geodesic.

Combining this with the phase determined above in Eq. (C7), we end up with an EM vector potential in the geometric optics approximation given by

$$(A_i) = \boldsymbol{A} = \boldsymbol{\mathcal{A}} e^{\mathrm{i}(k_0 ct \pm (1 - \frac{\gamma+1}{2}\frac{gz}{c^2})k_0 z)} + \mathcal{O}(\Gamma c^{-2}), \tag{C14}$$

where we introduce $\boldsymbol{\mathcal{A}} = (\mathcal{A}_x, \mathcal{A}_y, 0)$, and the electric scalar potential $-cA_0$ vanishes to our approximation. Note that we have now absorbed the factor ϵ^{-1} from the exponent of the ansatz [Eq. (C4)] into the normalization of k_0, such that the light's angular frequency as measured by a stationary observer at rest at the origin is again given by $\omega_0 = -ck_0$ as in the main text. Note also that this EM 4-potential satisfies (to our approximation) not only the Lorenz gauge condition under which it was derived, but also the "geometric Coulomb" gauge $\nabla_i A^i = 0$ (which is a somewhat sensible notion, given the $3+1$ split form of the metric): to our approximation, the difference term between the two gauge conditions is $\nabla_0 A^0 = \partial_0 A^0 + \Gamma^0_{0i} A^i + \cdots = \partial_0 A^0 + \frac{\bar\phi_{,i}}{c^2} A^i + \cdots$, and due to A^0, A^z, $\bar\phi_{,x}$, and $\bar\phi_{,y}$ vanishing in our approximation, this vanishes as well.

APPENDIX D: ATOM-LIGHT HAMILTONIAN

We now consider counterpropagating light fields that describe interaction processes in atom IFs—i.e., we define two light fields with temporal wave vector coefficients $k_{0,i}$, for $i = 1, 2$, corresponding to frequencies $\omega_{R,i} = -k_{0,i}c$, as measured by a resting observer at the origin. The coefficient appearing in the spatial component of the wave 4-vectors of the two light fields will be given by the $k_{0,i}$'s with opposite signs—i.e., for the first laser it will be positive and denoted by $k_{R,1} = |k_{0,1}| = \omega_{R,1}/c$; for the second one it will be negative and given by $-k_{R,2} = -|k_{0,2}| = -\omega_{R,2}/c$. We will add a time dependence to the amplitudes, as this will be used to create certain pulse shapes in the experiment, and write each of the corresponding vector potentials as

$$\boldsymbol{A}_i(z,t) = \boldsymbol{\mathcal{A}}_i(t) e^{\mathrm{i}\Phi_i(z,t)} + \mathcal{O}(\Gamma c^{-2}), \tag{D1}$$

where the phase expression is given by

$$\Phi_i(z,t) = -\omega_{R,i} t \pm \left(1 - \frac{\gamma+1}{2}\frac{gz}{c^2}\right) k_{R,i} z + \mathcal{O}(\Gamma c^{-2}), \tag{D2}$$

with $i = 1, 2$, respectively. Using canonical quantization, we write every motional variable with respect to the position and momentum operators $\hat Z$ and $\hat P$. Using the vector potential, we get expressions for the electric and magnetic fields via $\boldsymbol{E}_i(\hat Z, t) = -\partial_t \boldsymbol{A}_i(\hat Z, t)$ and $\boldsymbol{B}_i(\hat Z, t) = \nabla \times \boldsymbol{A}_i(\hat Z, t)$ as

$$\boldsymbol{E}_i(\hat Z, t) = \boldsymbol{\mathcal{E}}_i(t) e^{\mathrm{i}\Phi_i(\hat Z, t)} + \mathcal{O}(\Gamma c^{-2}), \tag{D3a}$$

$$\boldsymbol{B}_i(\hat Z, t) = \pm \boldsymbol{\mathcal{B}}_i(t) e^{\mathrm{i}\Phi_i(\hat Z, t)} + \mathcal{O}(\Gamma c^{-2}), \tag{D3b}$$

where the amplitudes are given by

$$\begin{aligned}\boldsymbol{\mathcal{E}}_i(t) &= -\mathrm{i}\omega_{R,i} \boldsymbol{\mathcal{A}}_i(t) - \dot{\boldsymbol{\mathcal{A}}}_i(t), \\ \boldsymbol{\mathcal{B}}_i(t) &= \mathrm{i} k_{R,i} \boldsymbol{e}_z \times \boldsymbol{\mathcal{A}}_i(t).\end{aligned}$$

The interaction Hamiltonian [Eq. (10)] then takes the form

$$\hat{H}_{\text{A-L}} = -\hat{\boldsymbol{d}}\cdot\boldsymbol{E}_i(\hat{Z},t) + \frac{1}{2m}[\hat{P}\cdot(\hat{\boldsymbol{d}}\times\boldsymbol{B}_i(\hat{Z},t)) + \text{H.c.}]. \tag{D4}$$

We now transform into the interaction picture corresponding to the internal Hamiltonian H_{I} in Eq. (8), which only alters the dipole operator

$$\hat{\boldsymbol{d}}(t) = e^{\mathrm{i}H_{\text{I}}t/\hbar}\hat{\boldsymbol{d}}e^{-\mathrm{i}H_{\text{I}}t/\hbar} = \boldsymbol{d}_{\text{eg}}|e\rangle\langle g|e^{\mathrm{i}\omega_{\text{eg}}t} \tag{D5}$$

with $\boldsymbol{d}_{\text{eg}} = \langle e|\hat{\boldsymbol{d}}|g\rangle$. Note that in order to commute the $\hat{Z}$-dependent phase of the magnetic field in the Röntgen term past the $\hat{P}$, we will use the relation $e^{\pm\mathrm{i}k\hat{Z}}\hat{P} = (\hat{P}\mp\hbar k)e^{\pm\mathrm{i}k\hat{Z}}$ (cf. [91]). We also use the Graßmann identity to simplify $(\boldsymbol{d}_{\text{eg}}\times(\boldsymbol{e}_z\times\boldsymbol{\mathcal{A}}_j))_z = \boldsymbol{d}_{\text{eg}}\cdot\boldsymbol{\mathcal{A}}_j$.

The full Hamiltonian, written in the rotating wave approximation and in the interaction picture with respect to $\hat{H}_{\text{I}}$, takes the form

$$\hat{H} = \hat{H}_{\text{M}} + \sum_i \frac{\hbar\Omega_i(\hat{Z},\hat{P},t)}{2}|\text{e}\rangle\langle\text{g}|e^{\mathrm{i}(\pm k_i(\hat{Z})\hat{Z}-(\omega_{R,i}-\omega_{\text{eg}})t)}, \tag{D6}$$

where the Rabi frequency has an additional dependency on the momentum

$$\frac{\hbar\Omega_i(\hat{P},t)}{2} = -\boldsymbol{d}_{\text{eg}}\cdot\boldsymbol{\varepsilon}_i\mathcal{E}_i(t) \pm (\hat{P}\mp\hbar k_{R,i}/2)\frac{\boldsymbol{d}_{\text{eg}}\cdot\boldsymbol{\varepsilon}_i}{m}\mathcal{B}_i(t),$$

and the coordinate wave vector is given by

$$k_i(\hat{Z}) = \left(1-(\gamma+1)\frac{g}{c^2}\hat{Z}\right)k_{R,i} + \mathcal{O}(c^{-4}). \tag{D7}$$

The nonrelativistic part of the $\hat{Z}$-dependent exponential of the Hamiltonian in Eq. (D6) is just the momentum translation

$$e^{\pm\mathrm{i}k_{R,i}\hat{Z}} = \int \mathrm{d}p|p\pm\hbar k_{R,i}\rangle\langle p|, \tag{D8}$$

whereas we now also have an additional contribution, $\exp(\pm\mathrm{i}\alpha k_{R,i}\hat{Z}^2)$ with $\alpha = -(\gamma+1)\frac{g}{c^2}$. Since this operator will act on spatially well-defined Gaussian wave packets, it is clear that the full operator $\exp(\pm\mathrm{i}(1+\alpha\hat{Z})k_{R,i}\hat{Z})$ will map a momentum eigenstate $|p\rangle$ to $|p\pm\hbar k_{R,i}(1+\alpha z)\rangle$, where z is the expectation value of $\hat{Z}$ with respect to the initial wave packet.

1. Doppler effect

Since we want to include all relativistic effects in atom IFs, including terms of the order c^{-2}, we need to consider not only the first-order Doppler effect, but also the second-order. Consider an atom-light interaction where the atoms have a velocity of v as measured in the lab frame. Note that a distinction between coordinate and proper velocity is not needed here, since both notions will differ by $\mathcal{O}(c^{-2})$ terms, which will manifest at the $\mathcal{O}(c^{-3})$ level for the first-order Doppler effect.

The light fields' frequencies will subsequently be perceived by the atoms as Doppler-shifted, characterized by $(1\mp\frac{v}{c}+\frac{v^2}{2c^2})\omega_{R,i}$, where the "+" corresponds to the first laser, moving upward, and vice versa. The wave vectors will, analogously, be shifted as $\pm(1\mp\frac{v}{c}+\frac{v^2}{2c^2}-(\gamma+1)\frac{gz}{c^2})k_{R,i}$. In order to compensate this Doppler shift, one has to rescale the laser frequencies inversely—i.e.,

$$\omega_{R,1} \mapsto \tilde{\omega}_{R,1}(v) = \left(1+\frac{v}{c}-\frac{v^2}{2c^2}+(\gamma+1)\frac{gz}{c^2}\right)\omega_{R,1},$$
$$\omega_{R,2} \mapsto \tilde{\omega}_{R,2}(v) = \left(1-\frac{v}{c}-\frac{v^2}{2c^2}+(\gamma+1)\frac{gz}{c^2}\right)\omega_{R,2},$$

where the gravitational contribution was discussed previously and needs to be adjusted in order to resonantly induce a momentum kick of $\hbar(k_{R,1}+k_{R,2}) = \hbar k_R$.

2. Bragg scattering matrix and effective laser phase

We can see that relativistic effects enter the atom-light interaction as corrections to the imprinted phase and momentum to the atoms. Those corrections consist (apart from the well-known first-order Doppler shift) of the second-order Doppler shift and a gravitational contribution. Similarly to [80,92], one can now understand Bragg transitions in terms of scattering matrices between atomic momentum eigenstates, as in Eq. (32), but now using the Doppler-corrected phase from Eq. (35). We are now able to write down an expression for the imprinted laser phase of the Bragg transition at each interaction event ($z_{\text{int}} = z$, $v_{\text{int}} = v$) as

$$\begin{aligned}\Phi_L(z,v) &= \pm(\Phi_1(z,v,\Delta t_1) - \Phi_2(z,v,\Delta t_2)) \\ &= \pm\left[\left(1+\frac{\gamma+1}{2}\frac{gz}{c^2}-\frac{v^2}{2c^2}\right)k_R + \frac{v}{c}\frac{\omega_R}{c}\right]z \\ &\quad \pm \Phi_{\text{FSL}}(v,\Delta t_1,\Delta t_2),\end{aligned} \tag{D9}$$

where Δt_i is the photon flight time from emission to interaction of the light field i, the sign corresponds to net momentum gain or loss, and we subsume the temporal parts of Eq. (D2) into

$$\Phi_{\text{FSL}}(v,\Delta t_1,\Delta t_2) = -\tilde{\omega}_{R,1}(v)\Delta t_1 + \tilde{\omega}_{R,2}(v)\Delta t_2. \tag{D10}$$

3. Finite-speed-of-light corrections

Let us summarize which FSL effects the Python code in [33] will neglect. Consider a light field which is emitted at a time t_{emit} and interacts with the atom at $t_{\mathrm{int}} = t_{\mathrm{emit}} + \Delta t$:

(1) The temporal part of the phase for each single-photon interaction, or analogously, the contribution Φ_{FSL} in Eq. (D10) in a two-photon process, will not be included in the laser phase, since it is directly proportional to the respective photon flight times.
(2) The spatial part of the phase $\Phi_L(z,\dot{z})$ in Eq. (34) needs to be evaluated at $\Phi_L(z(t_{\mathrm{int}}),\dot{z}(t_{\mathrm{int}}))$ and not at $\Phi_L(z(t_{\mathrm{emit}}),\dot{z}(t_{\mathrm{emit}}))$.
(3) The integration limits in the propagation phase integrals need to be shifted $t_{\mathrm{emit}} \mapsto t_{\mathrm{int}}$.
(4) The velocity v in the Doppler effect—i.e., the atomic velocity—needs to be evaluated as $v = \dot{z}(t_{\mathrm{int}})$, and not as $v = \dot{z}(t_{\mathrm{emit}})$.

Note that the first of these four effects is by far the biggest, since the phase of an EM wave is oscillating fast, even on timescales of Δt. The other three contributions directly depend on the atomic position/velocity difference between emission and interaction time, which is rather small due to the slow atomic velocity. We will comment on those approximations further in Appendix E in the analysis of an explicit Mach-Zehnder-type IF of [32].

APPENDIX E: MACH-ZEHNDER IF: COMPARISON TO DIMOPOULOS *ET AL.*

The papers [31,32] described a Raman matter wave IF of a Mach-Zehnder type in the PPN spacetime. In order to compare our results to their findings, we need to adapt their notation to ours. We list all needed differences in sign conventions and notation in Table III. Note that due to a different sign convention in the phases of the EM waves, one needs to redefine $\boldsymbol{k}_i \mapsto -\boldsymbol{k}_i$ and $\omega_i \mapsto -\omega_i$ for $i = 1, 2$, which gives an overall sign change in ω_R but not in k_R. However, some differences remain, even after aligning the notation. Dimopoulos *et al.* chose an initial height of $z_0 = 0$, and they included various FSL effects. Note that we assumed that the gravitational parameters g, Γ, and Λ are obtained by evaluating the gravitational potential and their derivatives in the original coordinate system, cf. Eq. (2). It could, however, also be the case that Dimopoulos *et al.* chose to evaluate those parameters using metric lengths and not coordinate lengths, which would shift those definitions by some factors of ϕ_0/c^2.

TABLE III. Comparison of notation between the analysis by Dimopoulos *et al.* [31,32] and this work.

Dimopoulos *et al.*	Our notation
g	$-(1+2\gamma\frac{\phi_0}{c^2})g$
$\partial_r g$	$(1+3\gamma\frac{\phi_0}{c^2})\Gamma$
$\partial_r^2 g$	$-\frac{1}{2}\Lambda$
T	T_R
ω_a	0
κ_{eff}	k_R
ω_{eff}	$-\omega_R$
v_L	v_0

We therefore expect deviations of our results in comparison to [32] at order $\mathcal{O}(4)$. As mentioned before, our provided Python code does not include FSL effects for arbitrary IF geometries. We will now, however, show how to calculate the dominant parts of the FSL phases for the explicit setup proposed by Dimopoulos *et al.* and will elaborate on the orders of magnitude of other FSL effects. For this, we will assume that the light fields will be emitted at the heights z_{low} and z_{up}. Note that for 10 m baselines, the maximal flight time for photons is therefore $\Delta T < 10^{-7}$ s.

FSL terms of first order. The biggest FSL contribution is the neglected temporal part of the phase of each EM field—i.e., the terms given by Eq. (D10). To evaluate this, we need to know the photonic flight time between emission and interaction. In order to keep the formulas short, we will explain the derivation using nonrelativistic trajectories.

Let us denote the interaction heights of the upper path by z_0 and $z_{u1} = z_0 + v_0 T_R - \frac{1}{2} g T_R^2 + \frac{\hbar k_R}{m} T_R$, and those of the lower path by $z_{l1} = z_0 + v_0 T_R - \frac{1}{2} g T_R^2$ and $z_2 = z_0 + 2v_0 T_R - 2g T_R^2 + \frac{\hbar k_R}{m} T_R$. We also depict these trajectories abstractly in Fig. 3. We can then write down the propagation times for each photon abstractly [93] as $\overline{\Delta t}_i^{(t_j)}$ for the upper atomic path and $\underline{\Delta t}_i^{(t_j)}$ for the lower atomic path,

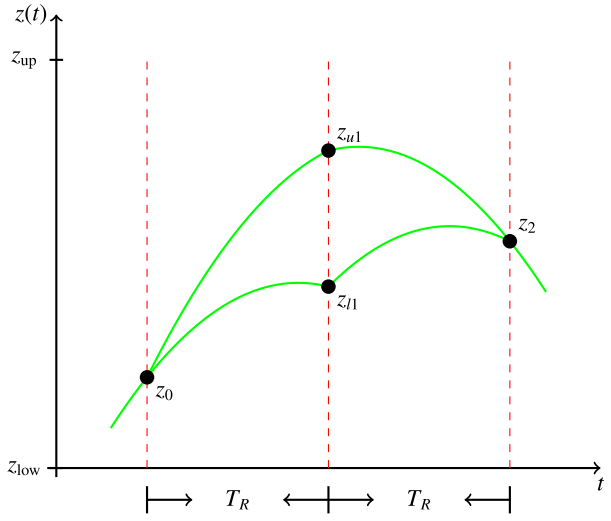

FIG. 3. Graphical description of interaction points (black dots) of photon paths (red dashed lines) and atoms (green solid lines) in the laboratory frame. The photon flight times are then defined by the emission height of z_{up} or z_{low} and the interaction points.

TABLE IV. Comparison of phase shifts for a Mach-Zehnder IF of our results and Dimopoulos *et al.* Factors of $\hbar$ and c are restored and highlighted in bold text. Cells which are highlighted gray coincide between our results and those of Dimopoulos *et al.* One can see that all terms of orders $\mathcal{O}(2)$ and $\mathcal{O}(3)$ are reproduced, apart from terms #8 and #9. The prefactors in terms #10 and #15 are also included, since the contribution of $\frac{7}{6}$ results from adding the Λ-dependent part of the gravitational potential to the Lagrangian, which manifests in the propagation phase. The additional $-\frac{1}{36}$ results from taking into account this part of the potential in the Euler-Lagrange equation, resulting in altered atomic trajectories. The latter effect seems to be left out in [32]. The comment "FSL" marks the first-order FSL effect described before.

Comparison to the Mach-Zehnder IF from [32]						
# in [32]	Original term in [32]	[32] in our notation	[32] in dimensionless parameter mod ω_C	Our result	$\mathcal{O}(n)$	Comment
1	$-\kappa_{\mathrm{eff}} g T^2$	$\kappa_R g T_R^2$	$\mathcal{R}_R \mathcal{G}_{1,R} T_R$	$\mathcal{R}_R \mathcal{G}_{1,R} T_R$	2	
2	$-\kappa_{\mathrm{eff}} (\partial_r g) v_L T^3$	$-\kappa_R \Gamma v_0 T_R^3$	$-\mathcal{R}_R \mathcal{G}_{2,R} \mathcal{V}_0 T_R$	$-\mathcal{R}_R \mathcal{G}_{2,R} \mathcal{V}_0 T_R$	3	
3	$-\frac{7}{12} \kappa_{\mathrm{eff}} (\partial_r g) g T^4$	$\frac{7}{12} \Gamma g \kappa_R T_R^4$	$\frac{7}{12} \mathcal{R}_R \mathcal{G}_{1,R} \mathcal{G}_{2,R} T_R$	$\frac{7}{12} \mathcal{R}_R \mathcal{G}_{1,R} \mathcal{G}_{2,R} T_R$	3	
4	$-3 \frac{\kappa_{\mathrm{eff}} g^2}{\boldsymbol{c}} T^3$	$-3 \frac{\kappa_R g^2}{c} T_R^3$	$-3 \mathcal{R}_R \mathcal{G}_{1,R}^2 T_R$	$-3 \mathcal{R}_R \mathcal{G}_{1,R}^2 T_R$	3	FSL
5	$-3 \frac{\kappa_{\mathrm{eff}} g v_L}{\boldsymbol{c}} T^2$	$3 \frac{\kappa_R g v_0}{c} T_R^2$	$3 \mathcal{G}_{1,R} \mathcal{V}_0 \mathcal{R}_R T_R$	$3 \mathcal{G}_{1,R} \mathcal{V}_0 \mathcal{R}_R T_R$	3	FSL
6	$-\frac{\hbar \kappa_{\mathrm{eff}}^2}{2m} (\partial_r g) T^3$	$-\frac{\hbar \kappa_R^2}{2m} \Gamma T_R^3$	$-\frac{1}{2} \mathcal{R}_R^2 \mathcal{G}_{2,R} T_R$	$-\frac{1}{2} \mathcal{R}_R^2 \mathcal{G}_{2,R} T_R$	3	
7	$(\omega_{\mathrm{eff}} - \omega_a) \frac{g T^2}{\boldsymbol{c}}$	$\omega_R \frac{g T_R^2}{c}$	$\mathcal{F}_R \mathcal{G}_{1,R} T_R$	$\mathcal{F}_R \mathcal{G}_{1,R} T_R$	2	FSL
8	$(2 - 2\beta - \gamma) \frac{\kappa_{\mathrm{eff}} g \phi T^2}{\boldsymbol{c^2}}$	$(2 - 2\beta + \gamma) \frac{\kappa_R g \phi_0 T_R^2}{c^2}$	$(2 - 2\beta + \gamma) \mathcal{G}_0 \mathcal{G}_{1,R} \mathcal{R}_R T_R$	$(2 - 2\beta + 2\gamma) \mathcal{G}_0 \mathcal{G}_{1,R} \mathcal{R}_R T_R$	3	PPN
9	$-\frac{3\hbar \kappa_{\mathrm{eff}}^2}{2m\boldsymbol{c}} g T^2$	$\frac{3\hbar \kappa_R^2}{2mc} g T_R^2$	$\frac{3}{2} \mathcal{R}_R^2 \mathcal{G}_{1,R} T_R$	$\frac{5}{2} \mathcal{R}_R^2 \mathcal{G}_{1,R} T_R$	3	FSL
10	$-\frac{7}{12} \kappa_{\mathrm{eff}} v_L^2 (\partial_r^2 g) T^4$	$\frac{7}{6} \kappa_R v_0^2 \Lambda T_R^4$	$\frac{7}{6} \mathcal{R}_R \mathcal{V}_0^2 \mathcal{G}_{3,R}$	$(\frac{7}{6} - \frac{1}{36}) \mathcal{R}_R \mathcal{V}_0^2 \mathcal{G}_{3,R}$	4	
11	$-\frac{35}{4\boldsymbol{c}} \kappa_{\mathrm{eff}} (\partial_r g) g v_L T^4$	$\frac{35}{4} \frac{\kappa_R \Gamma g v_0}{c} T_R^4$	$\frac{35}{4} \mathcal{R}_R \mathcal{V}_0 \mathcal{G}_{1,R} \mathcal{G}_{2,R} T_R$	$\frac{35}{4} \mathcal{R}_R \mathcal{V}_0 \mathcal{G}_{1,R} \mathcal{G}_{2,R} T_R$	4	FSL
12	$-\frac{4}{\boldsymbol{c}} \kappa_{\mathrm{eff}} (\partial_r g) v_L^2 T^3$	$-4 \frac{\kappa_R \Gamma v_0^2}{c} T_R^3$	$-4 \mathcal{R}_R \mathcal{V}_0^2 \mathcal{G}_{2,R} T_R$	$-4 \mathcal{R}_R \mathcal{V}_0^2 \mathcal{G}_{2,R} T_R$	4	FSL
13	$2 \frac{\omega_a g^2 T^3}{\boldsymbol{c^2}}$	0	0	0		Inelastic scattering
14	$2 \frac{\omega_a g v_L T^2}{\boldsymbol{c^2}}$	0	0	0		Inelastic scattering
15	$-\frac{7\hbar \kappa_{\mathrm{eff}}^2}{12m} v_L (\partial_r^2 g) T^4$	$\frac{7}{6} \frac{\hbar \kappa_R^2}{m} v_0 \Lambda T_R^4$	$\frac{7}{6} \mathcal{R}_R^2 \mathcal{V}_0 \mathcal{G}_{3,R}$	$(\frac{7}{6} - \frac{1}{36}) \mathcal{R}_R^2 \mathcal{V}_0 \mathcal{G}_{3,R}$	4	
$16 + 19$[a]	$[-12 g^2 + (2 - 2\beta - \gamma) \partial_r (g\phi)] \frac{\kappa_{\mathrm{eff}} v_L T^3}{\boldsymbol{c^2}}$	$-(14 - 2\beta - \gamma) \frac{\kappa_R g^2 v_0 T_R^3}{c^2}$	$-(14 - 2\beta - \gamma) \mathcal{R}_R \mathcal{G}_{1,R}^2 \mathcal{V}_0 T_R$	$(19 + 2\beta + 20\gamma) \mathcal{R}_R \mathcal{G}_{1,R}^2 \mathcal{V}_0 T_R$	4	PPN
$17 + 23$[a]	$[-7 - \frac{7}{12} (2 - 2\beta - \gamma)] \frac{\kappa_{\mathrm{eff}} g^3 T^4}{\boldsymbol{c^2}}$	$\frac{7}{12} (14 - 2\beta - \gamma) \frac{\kappa_R g^3 T_R^4}{c^2}$	$\frac{7}{12} (14 - 2\beta - \gamma) \mathcal{R}_R \mathcal{G}_{1,R}^3 T_R$	$-\frac{151 + 4\beta + 117\gamma}{12} \mathcal{R}_R \mathcal{G}_{1,R}^3 T_R$	4	PPN
18	$-5 \frac{\kappa_{\mathrm{eff}} g v_L^2 T^2}{\boldsymbol{c^2}}$	$5 \frac{\kappa_R g v_0^2}{c^2} T_R^2$	$5 \mathcal{R}_R \mathcal{G}_{1,R} \mathcal{V}_0^2 T_R$	$-\frac{11 + 12\gamma}{2} \mathcal{R}_R \mathcal{G}_{1,R} \mathcal{V}_0^2 T_R$	4	PPN
20	$-\frac{7}{12} (4 - 4\beta - 3\gamma) \frac{\kappa_{\mathrm{eff}} \phi (\partial_r g) g}{\boldsymbol{c^2}} T^4$	$\frac{7}{12} (4 - 4\beta - 3\gamma) \frac{\kappa_R \phi_0 \Gamma g}{c^2} T_R^4$	$\frac{7}{12} (4 - 4\beta - 3\gamma) \mathcal{G}_0 \mathcal{G}_{1,R} \mathcal{G}_{2,R} \mathcal{R}_R$	$\frac{100\beta - 100 - 14\gamma}{12} \mathcal{G}_0 \mathcal{G}_{1,R} \mathcal{G}_{2,R} \mathcal{R}_R$	4	PPN
21	$(\omega_{\mathrm{eff}} - \omega_a) \frac{(\partial_r g) v_L T^3}{\boldsymbol{c}}$	$-\omega_R \frac{\Gamma v_0 T_R^3}{c}$	$-\mathcal{F}_R \mathcal{G}_{2,R} \mathcal{V}_0 T_R$	$-\mathcal{F}_R \mathcal{G}_{2,R} \mathcal{V}_0 T_R$	3	FSL
22	$\frac{7}{12} (\omega_{\mathrm{eff}} - \omega_a) \frac{(\partial_r g) g T^4}{\boldsymbol{c}}$	$\frac{7}{12} \omega_R \frac{\Gamma g T_R^4}{c}$	$\frac{7}{12} \mathcal{F}_R \mathcal{G}_{1,R} \mathcal{G}_{2,R} T_R$	$\frac{7}{12} \mathcal{F}_R \mathcal{G}_{1,R} \mathcal{G}_{2,R} T_R$	3	FSL
24	$\frac{7\hbar \kappa_{\mathrm{eff}}^2}{2m\boldsymbol{c}} (\partial_r g) v_L T^3$	$\frac{7\hbar \kappa_R^2}{2mc} \Gamma v_0 T_R^3$	$\frac{7}{2} \mathcal{R}_R^2 \mathcal{G}_{2,R} \mathcal{V}_0 T_R$	$-\frac{19}{6} \mathcal{R}_R^2 \mathcal{G}_{2,R} \mathcal{V}_0 T_R$	4	FSL
25	$\frac{27\hbar \kappa_{\mathrm{eff}}^2}{8m\boldsymbol{c}} (\partial_r g) g T^4$	$-\frac{27\hbar \kappa_R^2}{8mc} \Gamma g T_R^4$	$-\frac{27}{8} \mathcal{R}_R^2 \mathcal{G}_{1,R} \mathcal{G}_{2,R} T_R$	$\frac{65}{24} \mathcal{R}_R^2 \mathcal{G}_{1,R} \mathcal{G}_{2,R} T_R$	4	FSL
26	$\frac{\hbar \kappa_{\mathrm{eff}} \omega_a}{m\boldsymbol{c^2}} g T^2$	0	0	0		Inelastic scattering
27	$6(2 - 2\beta - \gamma) \frac{\kappa_{\mathrm{eff}} \phi g^2 T^3}{\boldsymbol{c^3}}$	$6(2 - 2\beta - \gamma) \frac{\kappa_R \phi_0 g^2 T_R^3}{c^3}$	$6(2 - 2\beta - \gamma) \mathcal{R}_R \mathcal{G}_0 \mathcal{G}_{1,R}^2$	$6(4 - 4\beta + \gamma) \mathcal{R}_R \mathcal{G}_0 \mathcal{G}_{1,R}^2$	4	FSL
28	$3(\omega_{\mathrm{eff}} - \omega_a) \frac{g^2 T^3}{\boldsymbol{c^2}}$	$-3\omega_R \frac{g^2 T_R^3}{c^2}$	$-3 \mathcal{F}_R \mathcal{G}_{1,R}^2 T_R$	$-3 \mathcal{F}_R \mathcal{G}_{1,R}^2 T_R$	3	
29	$3(\omega_{\mathrm{eff}} - \omega_a) \frac{g v_L T^2}{\boldsymbol{c^2}}$	$3\omega_R \frac{g v_0 T_R^2}{c^2}$	$3 \mathcal{F}_R \mathcal{G}_{1,R} \mathcal{V}_0 T_R$	$3 \mathcal{F}_R \mathcal{G}_{1,R} \mathcal{V}_0 T_R$	3	
30	$6(1 - \beta) \frac{\phi g v_L T^2}{\boldsymbol{c^3}} \kappa_{\mathrm{eff}}$	$-6(1 - \beta) \frac{\phi_0 g v_0 T_R^2}{c^3} \kappa_{\mathrm{eff}}$	$-6(1 - \beta) \mathcal{G}_0 \mathcal{G}_{1,R} \mathcal{V}_0 \mathcal{R}_R$	$-6(2 - 2\beta + \gamma) \mathcal{G}_0 \mathcal{G}_{1,R} \mathcal{V}_0 \mathcal{R}_R$	4	FSL

[a]Terms #16 + #19 and #17 + #23 can be combined and therefore share a row.

where $i = 1, 2$ indicates the first or second laser and t_j is the time of laser emission—i.e.,

$$\overline{\Delta t}_1^{(0)} = \frac{z_0 - z_{\mathrm{low}}}{c}, \qquad \overline{\Delta t}_2^{(0)} = \frac{z_{\mathrm{up}} - z_0}{c},$$
$$\overline{\Delta t}_1^{(T_R)} = \frac{z_{u1} - z_{\mathrm{low}}}{c}, \qquad \overline{\Delta t}_2^{(T_R)} = \frac{z_{\mathrm{up}} - z_{u1}}{c},$$
$$\underline{\Delta t}_1^{(T_R)} = \frac{z_{l1} - z_{\mathrm{low}}}{c}, \qquad \underline{\Delta t}_2^{(T_R)} = \frac{z_{\mathrm{up}} - z_{l1}}{c},$$
$$\underline{\Delta t}_1^{(2T_R)} = \frac{z_2 - z_{\mathrm{low}}}{c}, \qquad \underline{\Delta t}_2^{(2T_R)} = \frac{z_{\mathrm{up}} - z_2}{c}.$$

The FSL phase of first order is then the sum over all previously neglected terms Φ_{FSL} at each interaction point—i.e.,

$$\begin{aligned}\Phi_{\mathrm{FSL},1} = {} & \Phi_{\mathrm{FSL}}(v_{\mathrm{up}}(0), \overline{\Delta t}_1^{(0)}, \overline{\Delta t}_2^{(0)}) \\ & - \Phi_{\mathrm{FSL}}(v_{\mathrm{up}}(T_R), \overline{\Delta t}_1^{(T_R)}, \overline{\Delta t}_2^{(T_R)}) \\ & - [\Phi_{\mathrm{FSL}}(v_{\mathrm{low}}(T_R), \underline{\Delta t}_1^{(T_R)}, \underline{\Delta t}_2^{(T_R)}) \\ & - \Phi_{\mathrm{FSL}}(v_{\mathrm{low}}(2T_R), \underline{\Delta t}_1^{(2T_R)}, \underline{\Delta t}_2^{(2T_R)})].\end{aligned}$$

Here, v_{up} and v_{low} denote the atomic (coordinate) velocities of each respective path as a function of time. Again, this contribution needs to be added to or subtracted from the final phase shift, depending on whether momentum was gained or lost in the interaction. This contribution will be manually added in the Python code in order to compare our results with those of [32].

FSL terms of second order. The next-order FSL correction one needs to keep in mind is that the spatial part of the laser phase also needs to be evaluated at the correct interaction time and not at the time of laser emission. One will therefore make an error that corresponds to the additional movement of the atoms in the time ΔT and their resulting change of height—i.e., to correct for this neglection, we need to make the replacement $k_R z(T_R) \mapsto k_R z(T_R + \Delta T)$. Since $v_0 \approx g T_R \approx 10 \frac{\mathrm{m}}{\mathrm{s}}$ is roughly the maximal velocity of the atoms, the possible error will be bounded by $v_0 \Delta T < 10^{-6}$ m and needs to be accounted for in every laser interaction. Note that this length variation needs to be compared to the measurement uncertainty of the atomic position, which is analyzed in [71] for a satellite mission, and assumed to also be on the order of 10^{-6} m.

FSL terms of third order. The third-order FSL correction arises in the propagation phase. It stems from the fact that the integration limits of the action integral need to be adjusted for the correct flight times of the photons—i.e., they need to be accounted for according to $T_R + \Delta T$. For example, for the kinetic energy part of the Lagrangian, this correction would manifest as

$$\int_{T_R}^{\Delta T_{\mathrm{up}}} \frac{m}{2} v_{\mathrm{up}}(t)^2 \mathrm{d}t - \int_{T_R}^{\Delta T_{\mathrm{low}}} \frac{m}{2} v_{\mathrm{low}}(t)^2 \mathrm{d}t. \tag{E1}$$

This effect would then manifest for differences between the photon flight times of the upper and lower IF path, since common photon flight times would effect both IF arms identically. At a path separation of 10 cm, this would correspond to a time delay between the IF arms of at most 3×10^{-10} s.

FSL terms of fourth order. Lastly, the velocity used in the Doppler shift formulas needs to be adjusted. If we assume an additional atomic velocity of $g\Delta T < 10^{-6} \frac{\mathrm{m}}{\mathrm{s}}$, then this would manifest in the first-order Doppler shift, due to an additional factor of c^{-1}, at around 10^{-14}.

1. Phase shift comparison

The comparison of our results to those of [32] can be found in Table IV. To orders $\mathcal{O}(2)$ and $\mathcal{O}(3)$, all terms except #8 and #9 are reproduced, whereas term #8 may result from a different definition of g by Dimopoulos *et al.*, as discussed before. Term #9 appears to arise due to a discrepancy in the computation of FSL effects in [32], wherein atomic positions, and therefore the photonic propagation times, were calculated using the atomic trajectory without any momentum kicks. Notably, when the number of imprinted photon momenta is set to zero in our calculation of the atomic position in the FSL phase, the outcome aligns with the prefactor of $3/2$ as reported by Dimopoulos *et al.* We have included a comment in the Python algorithm [33] that highlights this particular aspect. At order $\mathcal{O}(4)$, differences were expected, for example, due to our neglect of FSL effects. Note that we also reproduce all terms of [[75], Table 1] which are nonzero for our system if we leave out Λ corrections to the atomic trajectory.

[1] L. Morel, Z. Yao, P. Cladé, and S. Guellati-Khélifa, Determination of the fine-structure constant with an accuracy of 81 parts per trillion, Nature (London) **588**, 61 (2020).

[2] R. H. Parker, C. Yu, W. Zhong, B. Estey, and H. Müller, Measurement of the fine-structure constant as a test of the standard model, Science **360**, 191 (2018).

[3] X. Wu, Z. Pagel, B. S. Malek, T. H. Nguyen, F. Zi, D. S. Scheirer, and H. Müller, Gravity surveys using a mobile atom interferometer, Sci. Adv. **5**, eaax0800 (2019).

[4] G. Rosi, L. Cacciapuoti, F. Sorrentino, M. Menchetti, M. Prevedelli, and G. Tino, Measurement of the gravity-field curvature by atom interferometry, Phys. Rev. Lett. **114**, 013001 (2015).

[5] R. P. del Aguila, T. Mazzoni, L. Hu, L. Salvi, G. M. Tino, and N. Poli, Bragg gravity-gradiometer using the $^1S_0$-$^3P_1$ intercombination transition of ^{88}Sr, New J. Phys. **20**, 043002 (2018).

[6] B. Fang, I. Dutta, P. Gillot, D. Savoie, J. Lautier, B. Cheng, C. L. G. Alzar, R. Geiger, S. Merlet, F. P. D. Santos, and A. Landragin, Metrology with atom interferometry: Inertial sensors from laboratory to field applications, J. Phys. Conf. Ser. **723**, 012049 (2016).

[7] Q. Beaufils, L. A. Sidorenkov, P. Lebegue, B. Venon, D. Holleville, L. Volodimer, M. Lours, J. Junca, X. Zou, A. Bertoldi, M. Prevedelli, D. O. Sabulsky, P. Bouyer, A. Landragin, B. Canuel, and R. Geiger, Cold-atom sources for the matter-wave laser interferometric gravitation antenna (MIGA), Sci. Rep. **12**, 19000 (2022).

[8] Z. Chen, G. Louie, Y. Wang, T. Deshpande, and T. Kovachy, Enhancing strontium clock atom interferometry using quantum optimal control, Phys. Rev. A **107**, 063302 (2023).

[9] A. Bertoldi, P. Bouyer, and B. Canuel, in *Handbook of Gravitational Wave Astronomy* (Springer, Singapore, 2021), pp. 1–43.

[10] B. Canuel, S. Abend, P. Amaro-Seoane, F. Badaracco, Q. Beaufils, A. Bertoldi, K. Bongs, P. Bouyer, C. Braxmaier, W. Chaibi *et al.*, ELGAR—A European laboratory for gravitation and atom-interferometric research, Classical Quantum Gravity **37**, 225017 (2020).

[11] C. Ufrecht, F. Di Pumpo, A. Friedrich, A. Roura, C. Schubert, D. Schlippert, E. M. Rasel, W. P. Schleich, and E. Giese, Atom-interferometric test of the universality of gravitational redshift and free fall, Phys. Rev. Res. **2**, 043240 (2020).

[12] D. Schlippert, J. Hartwig, H. Albers, L. L. Richardson, C. Schubert, A. Roura, W. P. Schleich, W. Ertmer, and E. M. Rasel, Quantum test of the universality of free fall, Phys. Rev. Lett. **112**, 203002 (2014).

[13] T. Damour, Theoretical aspects of the equivalence principle, Classical Quantum Gravity **29**, 184001 (2012).

[14] D. Colladay and V. A. Kostelecký, CPT violation and the standard model, Phys. Rev. D **55**, 6760 (1997).

[15] J. Coleman, MAGIS-100 at Fermilab, Proc. Sci. ICHEP2018 (**2019**) 021 [arXiv:1812.00482].

[16] S. Loriani, A. Friedrich, C. Ufrecht, F. Di Pumpo, S. Kleinert, S. Abend, N. Gaaloul, C. Meiners, C. Schubert, D. Tell *et al.*, Interference of clocks: A quantum twin paradox, Sci. Adv. **5**, eaax8966 (2019).

[17] A. Roura, C. Schubert, D. Schlippert, and E. M. Rasel, Measuring gravitational time dilation with delocalized quantum superpositions, Phys. Rev. D **104**, 084001 (2021).

[18] M. Zych, F. Costa, I. Pikovski, and Č. Brukner, Quantum interferometric visibility as a witness of general relativistic proper time, Nat. Commun. **2**, 1 (2011).

[19] A. Roura, Gravitational redshift in quantum-clock interferometry, Phys. Rev. X **10**, 021014 (2020).

[20] F. Di Pumpo, C. Ufrecht, A. Friedrich, E. Giese, W. P. Schleich, and W. G. Unruh, Gravitational redshift tests with atomic clocks and atom interferometers, PRX Quantum **2**, 040333 (2021).

[21] H. Müller, A. Peters, and S. Chu, A precision measurement of the gravitational redshift by the interference of matter waves, Nature (London) **463**, 926 (2010).

[22] P. Wolf, L. Blanchet, C. J. Bordé, S. Reynaud, C. Salomon, and C. Cohen-Tannoudji, Atom gravimeters and gravitational redshift, Nature (London) **467**, E1 (2010).

[23] P. Wolf, L. Blanchet, C. J. Bordé, S. Reynaud, C. Salomon, and C. Cohen-Tannoudji, Does an atom interferometer test the gravitational redshift at the Compton frequency?, Classical Quantum Gravity **28**, 145017 (2011).

[24] M. A. Hohensee and H. Müller, Significance of the Compton frequency in atom interferometry, arXiv:1107.1830.

[25] D. M. Giltner, R. W. McGowan, and S. A. Lee, Theoretical and experimental study of the Bragg scattering of atoms from a standing light wave, Phys. Rev. A **52**, 3966 (1995).

[26] P. J. Martin, B. G. Oldaker, A. H. Miklich, and D. E. Pritchard, Bragg scattering of atoms from a standing light wave, Phys. Rev. Lett. **60**, 515 (1988).

[27] M. Ben Dahan, E. Peik, J. Reichel, Y. Castin, and C. Salomon, Bloch oscillations of atoms in an optical potential, Phys. Rev. Lett. **76**, 4508 (1996).

[28] E. Peik, M. Ben Dahan, I. Bouchoule, Y. Castin, and C. Salomon, Bloch oscillations and an accelerator for cold atoms, Appl. Phys. B **65** (1997).

[29] F. Di Pumpo, C. Ufrecht, A. Friedrich, E. Giese, W. P. Schleich, and W. G. Unruh, Gravitational redshift tests with atomic clocks and atom interferometers, PRX Quantum **2**, 040333 (2021).

[30] F. Di Pumpo, A. Friedrich, A. Geyer, C. Ufrecht, and E. Giese, Light propagation and atom interferometry in gravity and dilaton fields, Phys. Rev. D **105**, 084065 (2022).

[31] S. Dimopoulos, P. W. Graham, J. M. Hogan, and M. A. Kasevich, Testing general relativity with atom interferometry, Phys. Rev. Lett. **98**, 111102 (2007).

[32] S. Dimopoulos, P. W. Graham, J. M. Hogan, and M. A. Kasevich, General relativistic effects in atom interferometry, Phys. Rev. D **78**, 042003 (2008).

[33] M. Werner and K. Hammerer, Dataset: Atom interferometers in weakly curved spacetimes using Bragg diffraction and Bloch oscillations (Research Data Repository of the Leibniz University Hannover, 2023), https://dx.doi.org/10.25835/jnh3eryx.

[34] D. Schlippert, C. Meiners, R. Rengelink, C. Schubert, D. Tell, É. Wodey, K. Zipfel, W. Ertmer, and E. Rasel, in *CPT and Lorentz Symmetry: Proceedings of the Eighth Meeting on CPT and Lorentz Symmetry* (World Scientific, Singapore, 2020), pp. 37–40.

[35] S. Dimopoulos, P. W. Graham, J. M. Hogan, M. A. Kasevich, and S. Rajendran, Atomic gravitational wave interferometric sensor, Phys. Rev. D **78**, 122002 (2008).

[36] S. M. Dickerson, J. M. Hogan, A. Sugarbaker, D. M. S. Johnson, and M. A. Kasevich, Multiaxis inertial sensing with long-time point source atom interferometry, Phys. Rev. Lett. **111**, 083001 (2013).

[37] M.-S. Zhan, J. Wang, W.-T. Ni, D.-F. Gao, G. Wang, L.-X. He, R.-B. Li, L. Zhou, X. Chen, J.-Q. Zhong *et al.*, ZAIGA:

Zhaoshan long-baseline atom interferometer gravitation antenna, Int. J. Mod. Phys. D **29**, 1940005 (2020).
[38] L. Badurina, E. Bentine, D. Blas, K. Bongs, D. Bortoletto, T. Bowcock, K. Bridges, W. Bowden, O. Buchmueller, C. Burrage *et al.*, Aion: An atom interferometer observatory and network, J. Cosmol. Astropart. Phys. 05 (2020) 011.
[39] P. K. Schwartz and D. Giulini, Post-Newtonian Hamiltonian description of an atom in a weak gravitational field, Phys. Rev. A **100**, 052116 (2019).
[40] P. K. Schwartz, Post-Newtonian description of quantum systems in gravitational fields, Doctoral thesis, Gottfried Wilhelm Leibniz Universität Hannover, 2020, https://dx.doi.org/10.15488/10085.
[41] V. J. Martínez-Lahuerta, S. Eilers, T. E. Mehlstäubler, P. O. Schmidt, and K. Hammerer, *Ab initio* quantum theory of mass defect and time dilation in trapped-ion optical clocks, Phys. Rev. A **106**, 032803 (2022).
[42] C. Brans and R. H. Dicke, Mach's principle and a relativistic theory of gravitation, Phys. Rev. **124**, 925 (1961).
[43] K. Nordtvedt, Jr. and C. M. Will, Conservation laws and preferred frames in relativistic gravity: II. Experimental evidence to rule out preferred-frame theories of gravity, Astrophys. J. **177**, 775 (1972).
[44] D. Giulini, A. Großardt, and P. K. Schwartz, Coupling quantum matter and gravity, in *Modified and Quantum Gravity*, Lecture Notes in Physics Vol. 1017, edited by C. Pfeifer and C. Lämmerzahl (Springer, Cham, 2023), Chap. 16, https://doi.org/10.1007/978-3-031-31520-6_16.
[45] C. M. Will, Gravitation theory, Sci. Am. **231**, 25 (1974).
[46] See, e.g., the discussion in Chap. 6 of [47] and Eq. (6.2.14) therein.
[47] R. M. Wald, *General Relativity* (University of Chicago Press, Chicago, 2010).
[48] B. Bertotti, L. Iess, and P. Tortora, A test of general relativity using radio links with the Cassini spacecraft, Nature (London) **425**, 374 (2003).
[49] A. S. Konopliv, S. W. Asmar, W. M. Folkner, Ö. Karatekin, D. C. Nunes, S. E. Smrekar, C. F. Yoder, and M. T. Zuber, Mars high resolution gravity fields from MRO, Mars seasonal gravity, and other dynamical parameters, Icarus **211**, 401 (2011).
[50] A. Fienga, J. Laskar, P. Kuchynka, H. Manche, G. Desvignes, M. Gastineau, I. Cognard, and G. Theureau, The INPOP10a planetary ephemeris and its applications in fundamental physics, Celest. Mech. Dyn. Astron. **111**, 363 (2011).
[51] A. Verma, A. Fienga, J. Laskar, H. Manche, and M. Gastineau, Use of MESSENGER radioscience data to improve planetary ephemeris and to test general relativity, Astron. Astrophys. **561**, A115 (2014).
[52] Note that in order to keep the treatment of the external EM field consistent, differently from the original discussion in [39] (and from the non-gravitational one in [53], on which the derivation in [39] is based), we need to treat the external EM field not as a dynamical variable, but as a background field in which the motion of the atom takes place. A detailed explanation and discussion of this point may be found in [[40], Chap. 4], and in [[44], Sec. 16.2.1.2, footnote 15].
[53] M. Sonnleitner and S. M. Barnett, Mass-energy and anomalous friction in quantum optics, Phys. Rev. A **98**, 042106 (2018).
[54] This follows from $\frac{i}{\hbar}[\hat{\boldsymbol{r}}\cdot\hat{\boldsymbol{p}}, H_1] = 2\frac{\hat{p}^2}{2\mu} - \frac{e^2}{4\pi\varepsilon_0}\frac{1}{|\hat{r}|} + \mathcal{O}(c^{-2})$, and taking the matrix element with respect to $|g\rangle$.
[55] T. Chiba and S. Kinoshita, Quantum clocks, gravitational time dilation, and quantum interference, Phys. Rev. D **106**, 124035 (2022).
[56] F. Di Pumpo, A. Friedrich, C. Ufrecht, and E. Giese, Universality-of-clock-rates test using atom interferometry with T^3 scaling, Phys. Rev. D **107**, 064007 (2023).
[57] We disregard further relativistic corrections relevant in strong magnetic fields, cf. Eq. (5.9) in Schwartz *et al.* [39].
[58] T. Morishima, T. Futamase, and H. M. Shimizu, The general relativistic effects on the magnetic moment in Earth's gravity, Prog. Theor. Exp. Phys. **2018**, 063B07 (2018).
[59] D. Venhoek, Analyzing "Magnetic moments in curved spacetime": Pitfalls in GR, arXiv:1804.09524.
[60] H. Nikolic, Can effective muon $g-2$ depend on the gravitational potential?, arXiv:1802.04025.
[61] M. Schilling, É. Wodey, L. Timmen, D. Tell, K. H. Zipfel, D. Schlippert, C. Schubert, E. M. Rasel, and J. Müller, Gravity field modelling for the Hannover 10 m atom interferometer, J. Geodes. **94**, 122 (2020).
[62] L. Zhou, Z. Xiong, W. Yang, B. Tang, W. Peng, K. Hao, R. Li, M. Liu, J. Wang, and M. Zhan, Development of an atom gravimeter and status of the 10-meter atom interferometer for precision gravity measurement, Gen. Relativ. Gravit. **43**, 1931 (2011).
[63] C. Overstreet, P. Asenbaum, J. Curti, M. Kim, and M. A. Kasevich, Observation of a gravitational Aharonov-Bohm effect, Science **375**, 226 (2022).
[64] G. Rosi, F. Sorrentino, L. Cacciapuoti, M. Prevedelli, and G. Tino, Precision measurement of the Newtonian gravitational constant using cold atoms, Nature (London) **510**, 518 (2014).
[65] A. Lezeik, D. Tell, K. Zipfel, V. Gupta, É. Wodey, E. Rasel, C. Schubert, and D. Schlippert, Understanding the gravitational and magnetic environment of a very long baseline atom interferometer, arXiv:2209.08886.
[66] E. Giese, A. Roura, G. Tackmann, E. M. Rasel, and W. P. Schleich, Double Bragg diffraction: A tool for atom optics, Phys. Rev. A **88**, 053608 (2013).
[67] H. Ahlers, H. Müntinga, A. Wenzlawski, M. Krutzik, G. Tackmann, S. Abend, N. Gaaloul, E. Giese, A. Roura, R. Kuhl, C. Lämmerzahl, A. Peters, P. Windpassinger, K. Sengstock, W. P. Schleich, W. Ertmer, and E. M. Rasel, Double Bragg interferometry, Phys. Rev. Lett. **116**, 173601 (2016).
[68] Note that the notion of simultaneity is well defined because of the metric being static.
[69] M. Kasevich and S. Chu, Atomic interferometry using stimulated Raman transitions, Phys. Rev. Lett. **67**, 181 (1991).
[70] P. Storey and C. Cohen-Tannoudji, The Feynman path integral approach to atomic interferometry: A tutorial, J. Phys. II (France) **4**, 1999 (1994).
[71] S. Loriani, C. Schubert, D. Schlippert, W. Ertmer, F. Pereira Dos Santos, E. M. Rasel, N. Gaaloul, and P. Wolf, Resolution of the colocation problem in satellite quantum tests of the universality of free fall, Phys. Rev. D **102**, 124043 (2020).
[72] A. Roura, Circumventing Heisenberg's uncertainty principle in atom interferometry tests of the equivalence principle, Phys. Rev. Lett. **118**, 160401 (2017).
[73] C. Overstreet, P. Asenbaum, T. Kovachy, R. Notermans, J. M. Hogan, and M. A. Kasevich, Effective inertial frame in

an atom interferometric test of the equivalence principle, Phys. Rev. Lett. **120**, 183604 (2018).
[74] G. D'Amico, G. Rosi, S. Zhan, L. Cacciapuoti, M. Fattori, and G. M. Tino, Canceling the gravity gradient phase shift in atom interferometry, Phys. Rev. Lett. **119**, 253201 (2017).
[75] J. M. Hogan, D. Johnson, and M. A. Kasevich, Light-pulse atom interferometry, arXiv:0806.3261.
[76] Y.-J. Tan, C.-G. Shao, and Z.-K. Hu, Finite-speed-of-light perturbation in atom gravimeters, Phys. Rev. A **94**, 013612 (2016).
[77] A. Peters, K. Y. Chung, and S. Chu, High-precision gravity measurements using atom interferometry, Metrologia **38**, 25 (2001).
[78] S. Wajima, M. Kasai, and T. Futamase, Post-Newtonian effects of gravity on quantum interferometry, Phys. Rev. D **55**, 1964 (1997).
[79] H. Müller, S.-w. Chiow, and S. Chu, Atom-wave diffraction between the Raman-Nath and the Bragg regime: Effective Rabi frequency, losses, and phase shifts, Phys. Rev. A **77**, 023609 (2008).
[80] J.-N. Siemß, F. Fitzek, S. Abend, E. M. Rasel, N. Gaaloul, and K. Hammerer, Analytic theory for Bragg atom interferometry based on the adiabatic theorem, Phys. Rev. A **102**, 033709 (2020).
[81] This is also evident from the upper index in Eq. (63) in Dimopoulos *et al.* [32].
[82] F. Fitzek, J.-N. Siemß, S. Seckmeyer, H. Ahlers, E. M. Rasel, K. Hammerer, and N. Gaaloul, Universal atom interferometer simulation of elastic scattering processes, Sci. Rep. **10**, 22120 (2020).
[83] S.-w. Chiow, T. Kovachy, H.-C. Chien, and M. A. Kasevich, $102\hbar k$ large area atom interferometers, Phys. Rev. Lett. **107**, 130403 (2011).
[84] B. Plotkin-Swing, D. Gochnauer, K. E. McAlpine, E. S. Cooper, A. O. Jamison, and S. Gupta, Three-path atom interferometry with large momentum separation, Phys. Rev. Lett. **121**, 133201 (2018).
[85] F. Fitzek, J.-N. Kirsten-Siemß, E. M. Rasel, N. Gaaloul, and K. Hammerer, Accurate and efficient Bloch-oscillation-enhanced atom interferometry, arXiv:2306.09399.
[86] G. D. McDonald and C. C. Kuhn, Space-time area in atom interferometry, arXiv:1312.2713.
[87] C. J. Bordé, Atomic interferometry with internal state labelling, Phys. Lett. A **140**, 10 (1989).
[88] A. Alibabaei, P. K. Schwartz, and D. Giulini, Geometric post-Newtonian description of massive spin-half particles in curved spacetime, Classical Quantum Gravity **40**, 235014 (2023).
[89] C. W. Misner, K. S. Thorne, and J. A. Wheeler, *Gravitation* (W. H. Freeman, San Francisco, 1973).
[90] F. Di Pumpo, A. Friedrich, A. Geyer, C. Ufrecht, and E. Giese, Light propagation and atom interferometry in gravity and dilaton fields, Phys. Rev. D **105**, 084065 (2022).
[91] M. Sonnleitner and S. M. Barnett, The Röntgen interaction and forces on dipoles in time-modulated optical fields, Eur. Phys. J. D **71**, 1 (2017).
[92] E. Giese, Mechanisms of matter-wave diffraction and their application to interferometers, Fortschr. Phys. **63**, 337 (2015).
[93] Note that here we assume that light rays are given by $z = ct$, which is only valid to leading order. To be correct to higher order, one would need to solve the geodesic equation. Relativistic corrections of order $\mathcal{O}(c^{-2})$ are, however, not of interest when considering effects that are naturally of order $\mathcal{O}(c^{-1})$.